

Kondo-Majorana coupling in Double Quantum Dots.

by

Jesús David Cifuentes Pardo

Advisor: Luis Gregorio Dias da Silva

MASTER OF SCIENCE

in

Instituto de Física

(Condensed Matter Physics)

UNIVERSIDADE DE SÃO PAULO

(R. do Matão, 1371 - Butantã, São Paulo)

February 28, 2019

© Jesús David Cifuentes Pardo 2017

Chapter 1

Abstract

Majorana zero modes (MZMs) appearing at the edges of topological superconducting wires are a promising platform for fault-tolerant quantum computation. Novel proposals use MZMs tunneling inside quantum dots (QDs) to implement quantum architectures because today's precise experimental control over the QD parameters offers the unique possibility of manipulating the Majoranas inside multi-dot systems. In addition, recent experimental works reporting the detection of such quasi-particles together with Kondo anomalies , including a recent paper published by the advisor of this dissertation and collaborators [1], set out to explore the interplay of such Majorana zero-modes with the Kondo effect. The simplest case where Majorana manipulation is possible is in a double quantum dot (DQD). This model shows several possibilities for manipulation of MZM, including different geometric couplings such as linear and T junctions. In this project we perform analytical (non-interacting) and numerical(interacting) quantum transport studies of the transition of the Majorana signature. By tuning the model parameters we show that it is possible to control the localization of the MZM inside the DQD and explore its interplay with the Kondo effect.

Chapter 2

Table of Contents

1 Abstract	2
2 Table of Contents	3
3 Introduction and Motivation:	
The Pursuit of Majorana Fermions in superconducting wires.	5
3.1 The Kitaev Chain	7
3.1.1 Topological phase transition	10
3.1.2 Non-abelian statistics	12
3.1.3 Real implementations of the Kitaev Chain	14
3.2 Detecting Majorana zero modes in quantum dots	16
3.2.1 Why double quantum dots?	18
3.3 Overview	18
4 Preliminaries	20
4.1 Transport in Quantum Dots (QDs)	20
4.2 The Anderson Model	22
4.3 The Kondo Effect	24
4.3.1 Kondo Effect in QDs	26
5 Coupling a QD with a Majorana chain	28
5.1 Model	28
5.2 Non-interacting QD coupled to Majorana chain	30
5.3 Kondo-Majorana physics	33
6 Conclusions	36
References	37
Bibliography	38
Appendices	
A Appendix	45

Chapter 2. Table of Contents

A.1	From the logarithmic discretization to the Wilson's chain.	45
A.2	Three peak appearance in the Double Quantum Dot model.	49
A.3	Initial DQD-Majorana Hamiltonian.	50

Chapter 3

Introduction and Motivation: The Pursuit of Majorana Fermions in superconducting wires.

"It started out with a toy model demonstration, and then I realized it was very good model. You don't understand the full implications until other people start thinking it is true and they observe the big picture [...] Now, that toy model is like Hydrogen atom for topological materials- it turned out to be the first example of topological quantum matter."

– F. Duncan M. Haldane

In 2001 Alexei Yu. Kitaev presented a toy model that could lead to the implementation of topological qubits [2], an innovative idea that promised to sort out the problem of high decoherence in quantum computation . Kitaev used the properties of an exotic quasi-particle bound at the edges of a superconducting wire. This "bound state" was cataloged as a "Majorana fermion", the iconic particle predicted by Ettore Majorana in the 1930s. Majoranas were initially proposed to be real field solution of the Dirac equation, which describes a fermion that is its own antiparticle[3]. Till these days, no fundamental particle with these characteristics has been observed. However, novel exciting proposals are oriented to search these particles at the boundaries of topological superconducting wires.

These "topological superconductors", belong to an emergent group of materials that experience phase transitions without passing through a symmetry breaking, meaning that they cannot be characterized by Landau theory. Instead, these phases of matter are described by a new type



Figure 3.1: Coffee→donut: adiabatic evolution

of order determined by topology. In mathematics, the word topology is used to describe non-local features of surfaces (or manifolds) that are preserved under smooth deformations. The cliché, but always educative, joke to explain this concept says that "Topologists cannot tell the difference between a donut and a coffee cup, since one of them can always be continuously deformed into the other through a sequence of smooth and small alterations" (Figure 3.1).¹ However it wouldn't be possible to topologically transform a soccer ball into a donut since no there is no way of putting a hole into the ball by performing smooth deformations. We then say that coffee and donuts are topologically equivalent to each other, but not to the ball.

The insight of topology into the field of condensed matter physics is the following. Those materials who are attributed a topological characterization are endowed with a characteristic stability under smooth deformations (or adiabatic evolutions). Moreover, they usually present exotic excitations at its boundaries . The most famous example of this behavior is the integer quantum hall effect (IQHE), which exhibits an insulating bulk with electron currents passing through the edges of the material. More importantly, the magnetic field defines conductive platoes representing different topological phases. This effect is so robust that it allowed to define with high precision a resistivity standard unit $R_K = \frac{h}{e^2} = 25812.807557(18)\Omega$, which had major impact in science and technology.

Kitaev's toy model describes a one dimensional topological chain. Similar to the IQHE, this chain exhibits bizarre edge states, which are documented as bounded Majorana quasi-particles . Besides topological protection, these Majoranas have another important characteristic. They are non-abelian anyons [?]. This means that if we have three Majorana fermions γ_1, γ_2 and γ_3 and we, somehow, get to exchange the first two Majoranas and then we the second and the third, it produces a different state than exchanging the last two Majoranas first and then the first two. This is a very interesting property for quantum computing since it allows to encode information in many body systems. Kitaev pointed out that the combination of these two properties of Majoranas, topological stability and non-abelian statistics, could lead to the implementation of fault-tolerant quantum computers . This marked the beginning of a new area called topological quantum computing [4], which combines areas as different as topology, knot theory [5] and condensed matter physics.

These ideas motivated the pursuit of Majorana fermions in condensed matter systems [6–9]. Indeed, the last decade have been full of excitement, as new experiments have turned some of the theoretical predictions of the 1990s and 2000s into a reality. Very recently the first evidence of Majorana end states in TS has been found in multiple experiments [10–14] following the prescription by Oreg et al. [15] and Lutchyn et al. [16]. These experiments have been based on tunneling spectroscopy in junctions between TS and non metallic (NM) leads, where resonances have been observed at zero energy, consistent with the presence of Majorana zero-energy modes.

In the following section we will present a review of the main ideas behind the Kitaev chain (section section 3.1) taking special attention on its topological characterization and non-abelian

¹For decades, this has been the main reason for the absence of donuts at topology workshops.

statistics. Finally we will tell how that model inspired real implementations of Majorana wires in subsection 3.1.3. This discussion will eventually bring us closer to the main motivation of this thesis which is taken in the next section: The detection Majorana zero modes using quantum dots.

3.1 The Kitaev Chain

Kitaev's tight binding toy model represents an spinless superconducting chain with the following Hamiltonian

$$H = \sum_{i=1}^N \left[-t(a_i^\dagger a_{i+1} + a_{i+1}^\dagger a_i) - \mu a_i^\dagger a_i + \Delta a_i a_{i+1} + \Delta^* a_{i+1}^\dagger a_i^\dagger \right]. \quad (3.1)$$

Where μ is the chemical potential, so that $\mu a_i^\dagger a_i$ is the energy associated to each step in the chain, and $t(a_i^\dagger a_{i+1} + a_{i+1}^\dagger a_i)$ represents the interaction between neighboring sites which is determined by the hopping term t . The remaining terms describe the superconducting properties of the system as it is established by the BCS theory of superconductivity. Here, Δ is a complex superconducting parameter with the form $\Delta = e^{i\theta} |\Delta|$. The associated terms represent the Cooper pairs which can be created or annihilated at neighboring sites of the system hence breaking particle number. However, the system still preserves fermion parity, a property that will be very important during the rest of the project.

There are different ways to diagonalize this Hamiltonians. The usual method is to perform a Bogoliubov-de Gennes transformation which makes the problem equivalent to diagonalize a $2N \times 2N$ -matrix. However, Kitaev's brilliant solution passes through another transform. Lets define the operators $\gamma_{A,j}$ and $\gamma_{B,j}$ such that

$$\gamma_{A,j} = e^{i\theta/2} a_j + e^{-i\theta/2} a_j^\dagger, \quad \gamma_{B,j} = -i(e^{i\theta/2} a_j - e^{-i\theta/2} a_j^\dagger). \quad (3.2)$$

It is simple check that these operators are self-adjoint ($\gamma_{A,j}^\dagger = \gamma_{A,j}$, $\gamma_{B,j}^\dagger = \gamma_{B,j}$), which implies that they are their own antiparticle. Moreover, they satisfy the fermion anti-commutation relations

$$\begin{aligned} \{\gamma_{A,i}, \gamma_{A,j}\} &= \{\gamma_{B,i}, \gamma_{B,j}\} = 2\delta_{ij}, \\ \{\gamma_{A,i}, \gamma_{B,j}\} &= 0. \end{aligned} \quad (3.3)$$

These relations are characteristic from a Clifford algebra, which basically describes a fermion which is its own antiparticle. A Majorana fermion. Thus, we can think $\gamma_{A,i}, \gamma_{B,i}$ as Majorana operators.

Taking the inverse of (3.2) we obtain that each (Dirac) fermion in Hamiltonian (3.1) is composed by two Majorana fermions such that

$$a_j = \frac{e^{-i\theta/2}}{2} (\gamma_{A,j} + i\gamma_{B,j}), \quad a_j^\dagger = \frac{e^{i\theta/2}}{2} (\gamma_{A,j} - i\gamma_{B,j}). \quad (3.4)$$

3.1. The Kitaev Chain

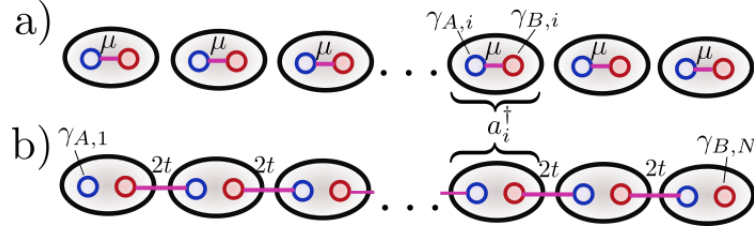


Figure 3.2: Illustration of the Kitaev chain for open boundary conditions in the Majorana representation. Dirac fermions are depicted by the big globes. Each one of them contains two Majoranas (small blue and red circles) a)Represents the trivial case where the hopping and the superconducting term approaches to 0. b) The non-trivial topological phase. The coupling is produced between Majoranas in different Dirac fermions

Source: By the author

Hence, we could adventure to say that these Majorana operators are actually dividing the Dirac fermions into real(γ_A) and imaginary (γ_B) part ,the same way as complex numbers are a composite of two real numbers. This is just a possible interpretation to elucidate that each Dirac fermion is composed by two types of Majorana quasi-particles just as in Figure 3.2.

The new Kitaev Hamiltonian in the "Majorana representation" looks like

$$H = \frac{i}{2} \sum_{j=1}^N [-\mu \gamma_{A,j} \gamma_{B,j} + (t + |\Delta|) \gamma_{B,j} \gamma_{A,j+1} + (t - |\Delta|) \gamma_{A,j} \gamma_{B,j+1}] + \text{Const}, \quad (3.5)$$

Depending on the values of parameters μ, t and $|\Delta|$ we can identify two regimes represented by the following situations:

1. If $|\Delta| = t = 0$ and $\mu < 0$, Hamiltonian (3.5) becomes $\frac{-i\mu}{2} \sum_j \gamma_{A,j} \gamma_{B,j}$ which represents the coupling of the Majoranas in the same Dirac fermion. (See Figure 3.2 (a))
2. If $|\Delta| = t > 0$ and $\mu = 0$, the situation is much more interesting. The Hamiltonian (3.5) takes the form $H = 2ti \sum_j \gamma_{B,j} \gamma_{A,j+1}$. This implies that the coupling is performed between Majoranas of different Dirac fermions. Notably, this configuration leaves the edge Majorana operators ($\gamma_{A,1}$ and $\gamma_{B,N}$) uncoupled to the system (See Figure Figure 3.2b)). Note that these uncoupled Majorana fermions can be at any state without any repercussion in the energy of the system. This explains the emergence of a ground state localized at edges of the chain.

These two situations are representatives of two different topological phases. The trivial phase occurs for $\frac{\mu}{2t} > 1$ and the non-trivial phase appears when $\frac{\mu}{2t} < 1$ (See Figure 3.3). The mean characteristic of the non-trivial phase is the creation of a robust zero-mode generated by

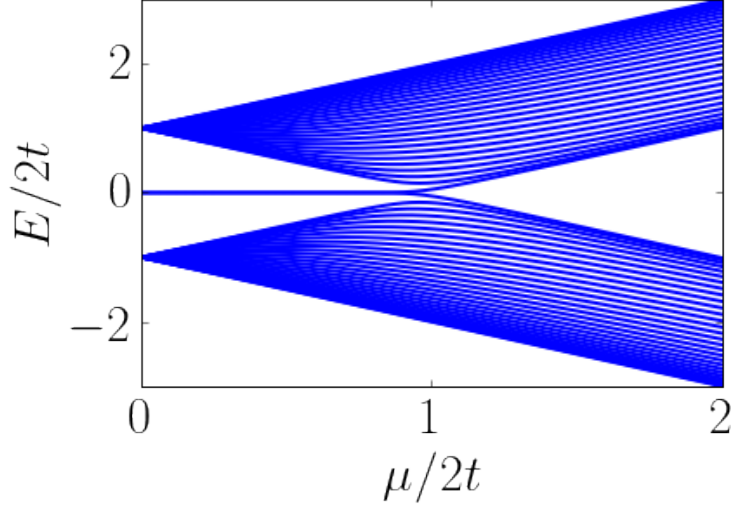


Figure 3.3: Spectrum of Hamiltonian 3.5 with 30 sites and $t = |\Delta|$ s. Method: Numerical diagonalization.

Source: By the author

the uncoupled Majorana fermions at the edges of the Kitaev chain. Note that if

$$H = 2ti \sum_j \gamma_{B,j} \gamma_{A,j+1}, \quad (3.6)$$

it is possible to define new Dirac fermion operators as

$$c_j = \frac{1}{\sqrt{2}} (\gamma_{B,j} + i\gamma_{A,j+1}), \quad c_j^\dagger = \frac{1}{\sqrt{2}} (\gamma_{B,j} - i\gamma_{A,j+1}).$$

Then (3.7) becomes

$$H = ti \sum_{j=1}^{N-1} (2c_j^\dagger c_j - 1). \quad (3.7)$$

Therefore, a ground state $|\Omega\rangle$ of this Hamiltonian is an state vacuum at all sites j from 1 to $N-1$ ($c_j|\Omega\rangle = 0$). This condition allows some degeneracy since the sites at the boundary are not coupled to the Hamiltonian $\gamma_{A,1}$ and $\gamma_{B,N}$. The Dirac operators formed by these Majoranas

$$c_N = \frac{1}{\sqrt{2}} (\gamma_{B,N} + i\gamma_{A,1}), \quad c_N^\dagger = \frac{1}{\sqrt{2}} (\gamma_{B,N} - i\gamma_{A,1}),$$

can be either occupied ($c_N^\dagger c_N|\Omega\rangle = 1$) or empty ($c_N^\dagger c_N|\Omega\rangle = 0$). Each of these results will have a different fermion parity, that is a symmetry of our Hamiltonian. Indeed, we can define a global parity operator as

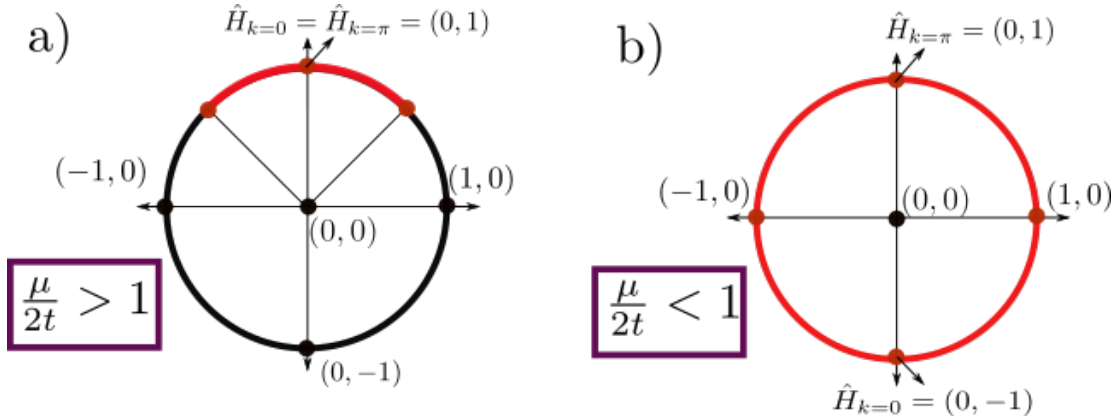


Figure 3.4: Path of \hat{H}_k for the interval $[-\pi, \pi]$. a) Trivial phase: The resulting path can be homotopically deformed to a point. b) Non-trivial phase: The path is a non-contractible loop around the unitary circle.

Source: By the author

$$\mathcal{D} = \prod_{i=1}^N \left(2c_j^\dagger c_j - 1 \right) = \prod_{i=1}^N -i\gamma_{B,j}\gamma_{A,j+1} = \pm 1. \quad (3.8)$$

In the ground state $|\Omega\rangle$, this parity will be defined by the result of $\gamma_{B,N}\gamma_{A,1}$ because the other states are fixed by $(c_j|\Omega\rangle = 0)$. This is an important point, since symmetry protection is actually correlating the two opposite sites of the Kitaev chain i.e. Any attempt to disturb one site of the chain would perturb the other site to guarantee the preservation of fermion parity. This is a great deal, it shows how coherent are these Majorana edge states. A possible explanation for this is the topology of the Kitaev chain, which is the objective of the next subsection.

3.1.1 Topological phase transition

Both regimes described previously can be characterized with a topological parameter. A didactic method to explain is the one used by Alicea[8]. First of all, suppose that we have an infinite Kitaev chain chain ($N = \infty$) in (3.5). This system is translation invariant, hence we can make a Fourier transformation to the momentum space as

$$H = \sum_{k \in BZ} (b'_k \ c'_k) H_k \begin{pmatrix} b'_{-k} \\ c'_{-k} \end{pmatrix}, \quad (3.9)$$

with the Bloch Hamiltonian equal to

$$H_k = \begin{pmatrix} 0 & \frac{-i\mu}{2} + it \cos k + |\Delta| \sin k \\ \frac{i\mu}{2} - it \cos k + |\Delta| \sin k & 0 \end{pmatrix} = (|\Delta| \sin k) \sigma_x + \left(\frac{\mu}{2} - t \cos k\right) \sigma_y. \quad (3.10)$$

Here, σ_x and σ_y are the corresponding Pauli matrices. The Brilloin zone (*BZ*) is the periodic space $[-\pi, \pi]$ which can be mapped to the unitary circle. Equation (3.10) determines the coordinates of the Bloch Hamiltonian in the base $\{\sigma_x, \sigma_y\}$.

We can map these coordinates to the unitary circle by taking the norm of this vector giving

$$\hat{H}_k = \frac{1}{\sqrt{|\Delta|^2 \sin^2 k + (\frac{\mu}{2} - t \cos k)^2}} \begin{pmatrix} |\Delta| \sin k \\ \frac{\mu}{2} - t \cos k \end{pmatrix}. \quad (3.11)$$

Note that $|\Delta|^2 \sin^2 k + (\frac{\mu}{2} - t \cos k)^2 \neq 0$ for all the values of k as long as $\frac{\mu}{2t} \neq 1$. When $\frac{\mu}{2t} = 1$ the $H_{k=0} = 0$, so it cannot be normalized. This is the same point were the phase transition occurs!. At any other value of $\frac{\mu}{2t}$ it is possible to normalize H_k for all values of $k \in BZ$. The result of mapping \hat{H}_k for all k is a path onto the unitary circle.

This path can take two forms as we can observe in Figure 3.4. If $\frac{\mu}{2t} > 1$ the path is an arc in the part of the circle. In the non-trivial phase $\frac{\mu}{2t} < 1$ the path completes a wind around the circle. This is a topological difference between both phases. While the path described by the trivial phase can be contracted to a single dot, the path described by the non-trivial circle is a circle that cannot be contracted. We can determine whether path of a given phase is of type a) or type b) we only need to check if $\hat{H}_{k=0}$ and $\hat{H}_{k=\pi}$ are the same point $(0, 1)$ or the opposite points $(0, 1)$ and $(0, -1)$. This transforms into a simple equation

$$\hat{H}_{k=0,y} \hat{H}_{k=\pi,y} = \begin{cases} 1 & \text{trivial phase} \\ -1 & \text{non-trivial phase} \end{cases} \quad (3.12)$$

where $\hat{H}_{k=0,y}$ is the y -th component of \hat{H}_k . The term $\hat{H}_{k,y}$ is a particular case of the Pfaffian $\mathcal{P}(k)$, which widely used to characterize topological phase transitions involving Majorana fermions.

In a more general perspective, the mean idea behind this topological characterization relies in the adiabatic theorem. In simple words, the adiabatic theorem says that a slow evolution of a gaped Hamiltonian will produce a smooth evolution of its eigenstates, so that the order of energies remains unchanged.

A keyword in the previous definition is "gaped". As we can observe in Figure 3.3 the phase transition occurs at $\frac{\mu}{2t} = 1$. This point is where the gap of the Hamiltonian closes. In periodic boundary conditions no Majorana zero modes will emerge since there are no edges in the system. Therefore, the edge states with zero energy for $\frac{\mu}{2t} < 1$ will not appear. We obtain that the gapless point $\frac{\mu}{2t} = 1$ divides two gapped regimes. According to the adiabatic theorem, these two regions must be separated, hence meaning that no adiabatic evolution could lead from one region to the other since that would involve crossing through a gapless Hamiltonian.

In conclusion, these gapless Hamiltonians are forbidden in an adiabatic evolution. The banned points can be thought as "holes" in the space of Hamiltonians, which generates spaces with non-trivial topologies. Since adiabatic evolutions can be understood as smooth deformations of the Hamiltonian, the relation with topology becomes clear. Thus, characterizing the phase transitions in the Kitaev chain, as in similar robust materials, is mainly a topological problem. This involves computing topological quantities such as Pfaffians, Chern numbers or Winding numbers, which are always integer values.

All of this, lead us to an interesting question. If we have two connected topological materials, one characterized by the number 0 and the other by the number 1, then what should happen at the boundary between these two discrete parameters?. Indeed some excitations are visible at the boundaries of topological materials. In the IQHE, these excitations are quantized currents passing through the edges of the placket. In the Kitaev chain these are the Majorana quasi-particles.

Finally, note that in a system that preserves symmetries, the space of Hamiltonians has more forbidden points. Therefore, these systems have different topological characterizations according to the protected symmetries [17]. This is the case of the Kitaev chain where the topological phase protects the parity of the symmetry under perturbations involving the two opposed Majoranas at the edges. This endowed topological stability combined with Majorana's non-abelian statistics (next subsection) makes the Kitaev chain a promising platform for quantum computation.

3.1.2 Non-abelian statistics

Imagine that we want to exchange two Majorana fermions γ_1 and γ_2 ². This procedure can be performed with an adiabatic evolution of the Hamiltonian $H(t)$ that exchanges both operators while leaving the system invariant. Therefore, after a period T we require that

$$\begin{aligned}\gamma_1(T) &\rightarrow \gamma_2(0) \\ \gamma_2(T) &\rightarrow \gamma_1(0)\end{aligned}\tag{3.13}$$

while $H(0) = H(T)$.

The adiabatic evolution is then represented by a unitary operator $U(t) = e^{-\frac{i}{\hbar} \int H(t)}$ and is applied according to Heisenberg's picture as

$$\gamma_i(T) = U^\dagger(t) \gamma_i U(t).$$

Since Majoranas preserve fermion parity, H must commute with the parity operator $P = -i\gamma_1\gamma_2$. In a Clifford algebra generated by the operators γ_1 and γ_2 (See algebraic relations (3.3)), $[H, \gamma_1\gamma_2] = 0$ implies that $H(t) \propto \gamma_1\gamma_2$ or $H(t)$ is a constant. Taking the non-trivial answer we obtain that the

²This section is inspired on the webpage topocondmat https://topocondmat.org/w2_majorana/braiding.html, which contains an amazing tutorial about Majorana fermions and topological condensed matter.

3.1. The Kitaev Chain

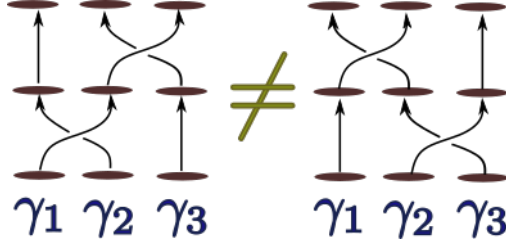


Figure 3.5: Representation of non-abelian braiding .

evolution operator has the form $U(t) = e^{\alpha(t)\gamma_1\gamma_2}$, where $\alpha(t)$ is a complex function over t . We can simplify this exponential noting that $(\gamma_1\gamma_2)^2 = -1$ which after Taylor expansion reduces to

$$U(t) = \cos(\alpha(t)) - \gamma_1\gamma_2 \sin(\alpha(t)). \quad (3.14)$$

Replacing this solution in (3.13) we obtain

$$\begin{aligned} \gamma_1(T) &= \gamma_1 \cos(2\alpha(T)) - \gamma_2 \sin(2\alpha(T)) \rightarrow \gamma_2 \\ \gamma_2(T) &= \gamma_2 \cos(2\alpha(T)) + \gamma_1 \sin(2\alpha(T)) \rightarrow \gamma_1, \end{aligned} \quad (3.15)$$

which can only happen if $\alpha(T) = \pm\frac{\pi}{4}$. Hence we conclude that the exchange operator between both Majoranas is

$$U_{12} = e^{\pm\frac{\pi}{4}\gamma_1\gamma_2} = \frac{1}{\sqrt{2}}(1 \pm \gamma_1\gamma_2). \quad (3.16)$$

Note that this exchange does not depend on the evolution, nor the period T .

Now imagine that we have three Majoranas γ_1, γ_2 and γ_3 and we want to perform the following processes. On the first one, we exchange Majoranas 1 and 2 and then the Majorana in 2 (which was initially at 1) is exchanged with Majorana 3 (Figure 3.5[Left]). On the second process, we invert the order, hence exchanging first exchange Majoranas 2 and 3 and then Majoranas 1 and 2 (Figure 3.5[Right]). These two cases are represented by the following operators respectively

$$\begin{aligned} U_{23}U_{12} &= \frac{1}{2}(1 + \gamma_2\gamma_3)(1 + \gamma_1\gamma_2) = \frac{1}{2}(1 + \gamma_2\gamma_3 + \gamma_1\gamma_2 + \gamma_3\gamma_1) \\ U_{12}U_{23} &= \frac{1}{2}(1 + \gamma_1\gamma_2)(1 + \gamma_2\gamma_3) = \frac{1}{2}(1 + \gamma_1\gamma_2 + \gamma_2\gamma_3 + \gamma_1\gamma_3). \end{aligned} \quad (3.17)$$

Since $\gamma_3\gamma_1 = -\gamma_1\gamma_3$, the outcome of both processes is essentially different, which means that it actually matters the order in which the Majoranas are exchanged .

The particles that satisfy this strange property receive the name of non-abelian anyons. While the word "anyon" usually integrates several types of particles including bosons and fermions, the word non-abelian makes emphasis on those anyons with non-commutative exchange statistics.

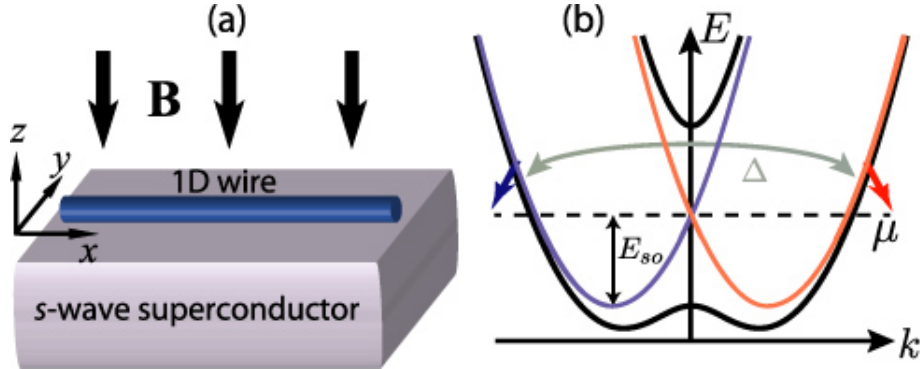


Figure 3.6: (a) Setup of a Majorana wire with high spin-orbit coupling, over a superconducting plane and an induced Zeeman field. (b) Splitting of the energy bands with different spins in the non-superconducting regime (red and yellow bands). With superconducting proximity , a gap is opened and the red and blue energy bands are projected forming the black bands.

Source: Adapted from [8]

Non-abelian statistics is what make anyons a fantastic candidate to implement quantum algorithms. The idea of exchanging anyons can be thought as a braiding code like in Figure 3.5. Since the order of braiding matters, different braiding orders can be associated to distinct algorithms. This generates another form of codifying information which has been extensively studied in knot theory [5]. And if these anyons were topological, they will be protected from quantum decoherence [18]. To the date, the closest candidates to satisfy both properties (non-abelian statistics and topological characterization) are the Majorana fermions. Nonetheless, the basic braiding protocol that would unleash the keys to topological quantum computation [4] has not been measured yet. Many theoretical proposals have been set up in this direction, but there is still a long experimental road.

3.1.3 Real implementations of the Kitaev Chain

One of the main problems to implement real devices capable to exhibit Majorana quasi-particles at the boundaries, is that Majorana's are spin-less. Since all materials have fermion doubling, it was necessary to endow the system with a physical property that could separate the spin energy bands. To bypass this problem, Lutchyn et al. proposed using a material with strong spin-orbit Rashba interaction [19] and applying a magnetic field. This would split the energy band by spin, hence destroying fermion doubling.

This idea allowed scientists to designed the first Majorana wires. The recipe consists in growing a semi-conducting wire with high spin-orbit coupling, over an s'wave superconductor and inducing a Zeeman magnetic field (Figure 3.6(a)). Such model is described by a Hamiltonian of the form [8](65)

3.1. The Kitaev Chain

$$H = H_{\text{wire}} + H_{\delta} \quad (3.18)$$

with

$$H_{\text{wire}} = \sum_{\sigma \in \{\uparrow, \downarrow\}} \int dx \psi_{\sigma}^{\dagger}(x) \left(\frac{-1}{2m} \partial_x^2 - \mu - i\alpha \sigma_y \partial_x + h \sigma_x \right) \psi_{\sigma}(x), \quad (3.19)$$

$$H_{\Delta} = \int dx \Delta \psi_{\downarrow} \psi_{\uparrow} + \Delta^* \psi_{\uparrow} \psi_{\downarrow}. \quad (3.20)$$

Where $\psi_{\sigma}^{\dagger}(x)$ creates a particle at x with spin σ , μ is the chemical potential, h is the Zeeman splitting energy and $\alpha > 0$ is the Rashba spin-coupling parameter, favoring spin-align. The induced superconducting proximity is depicted by H_{Δ} where Δ is the superconducting gap. Note that this system (3.18) has all the ingredients of the Kitaev chain.

If $\Delta = 0$, the Bloch Hamiltonian is given by

$$\mathcal{H}_k = \frac{k^2}{2m} - \mu + k\alpha \sigma_y + h \sigma_x. \quad (3.21)$$

And diagonalizing this matrix we obtain that the band splits as

$$\epsilon_{\pm}(k) = \frac{k^2}{2m} - \mu \pm \sqrt{(\alpha k)^2 + h^2} \quad (3.22)$$

with opposed spins as observed in the blue and red lines of Figure 3.6(b).

The superconducting proximity effect ($\Delta > 0$) opens a gap that projects the upper and lower bands forming the black bands of Figure 3.6(b). This separation of both energy channels allows us to think the conduction band as an spin-less. This system enters into the topological phase when

$$h > \sqrt{\Delta^2 + \mu^2}. \quad (3.23)$$

At these points, Majorana bound states emerge at the edges of the wire.

This theoretical proposal led in 2012 to the first observation of Majorana signatures in InSb nanowires ³, by Mourik et al. from the Kavli Institute at Delft. This was a huge boost to the field which immediately attracted abundant experimental and theoretical work.

In just 6 years, more than 5 groups have documented the observation of Majorana signatures [11–14, 20]. This signature is characterized by the emergence of a robust zero bias conductance peak ZBCP of height $\frac{2e^2}{h}$ produced by the Majorana zero mode MZM localized at the edges of the wire. Though the first experiments didn't observed such an stable signature, the last year Zhang et al. published a paper documenting the observation of this robust peak with the expected theoretical magnitude in and InSb wire Figure 3.7. As can be observed in Figure 3.7(b)

3.2. Detecting Majorana zero modes in quantum dots

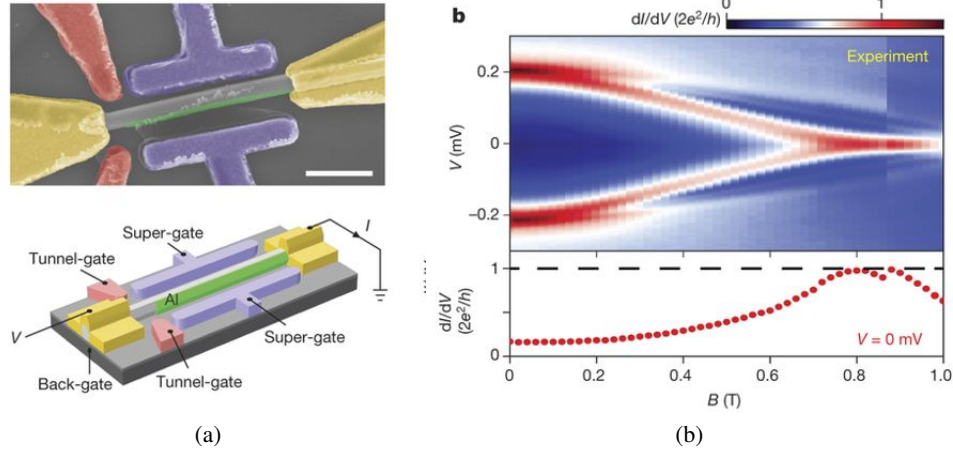


Figure 3.7: (a) Experimental setup (b) Observed magnetic field dependence of the zero bias peak.

Source: [14]

the ZBCP increases up to $\frac{2e^2}{h}$ for a strong magnetic field, where the system enters the topological phase according to equation (3.23).

Despite the successful experimental results, there is still certain skepticism about the existence of Majorana fermions, mainly because Majorana zero-modes (MZM) have been found in superposition with similar types of phenomena that produce zero-modes. Some examples of these are the Andreev reflection [21] or even the Kondo peak [22]. New experimental proposals focus on distinguishing MZMs from these effects and implementing braiding protocols [23–25]. One promising idea that could lead to important results in both research lines is coupling Majorana wires with QDs. This will be the objective of the following section.

3.2 Detecting Majorana zero modes in quantum dots

Liu and Baranger were the first to propose in 2011 the possibility of using QDs to detect Majorana zero modes [26]. When a QD is attached to the end of a Majorana chain in the topological phase, the Majorana Zero Mode at the end of the chain leaks inside the QD [27] producing a zero-bias conductance peak of half a quanta $\frac{e^2}{2h}$ through the dot. This method of detecting Majorana signatures presents important advantages:

- 1. It does not destroy the entire qubit information:** Other detection methods such as tunneling spectroscopy have the downside that it probes not only the end of the Topological

³A material with strong spin-orbit coupling and large g factor.

3.2. Detecting Majorana zero modes in quantum dots

Superconductor(TS), but its bulk as well. This completely destroys the qubit information. When attaching the Majorana chain to a QD it is the conductivity is measured through the QD which does not disturb the bulk of the chain.

2. **Kondo-Majorana physics:** The observation of Kondo signatures in superconducting devices [28] and the similarities between Kondo and Majorana signatures [27] motivated to study the existence of prospective Kondo-Majorana physics [22, 29]. These two effects could co-exist at temperatures of a few mili-kelvins in quantum impurity systems.

Quantum dots (QD) are artificial and adaptable quantum impurities, which makes them the best device to perform this kind of study. In particular, a QD-Majorana system was already studied by my advisor in a previous paper [1], where he proofed that it is possible separate Kondo and Majorana physics by tuning dot's gate voltage or by applying a strong magnetic field.

3. **Manipulation of Majorana zero modes:** Today's precise experimental control over QDs makes us dream with the possibility of implementing scalable braiding proposals Figure 3.8(a) and quantum architectures for topological quantum computation Figure 3.8(b).

These architectures perform adiabatic evolutions similar to the ones described in subsection 3.1.2 to braid Majorana fermions. This operation strongly relies on the possibility of manipulating the Majorana zero modes inside the dots. The main idea of MZM manipulation is to tune the gate voltage of one dot to induce the Majoranas to "move" into the other dots. In a prospective braiding protocol, as the one described in [30] (Figure 3.8(a)), this manipulation process would have to be performed several times. However, till this moment MZM manipulation hasn't been achieved experimentally.

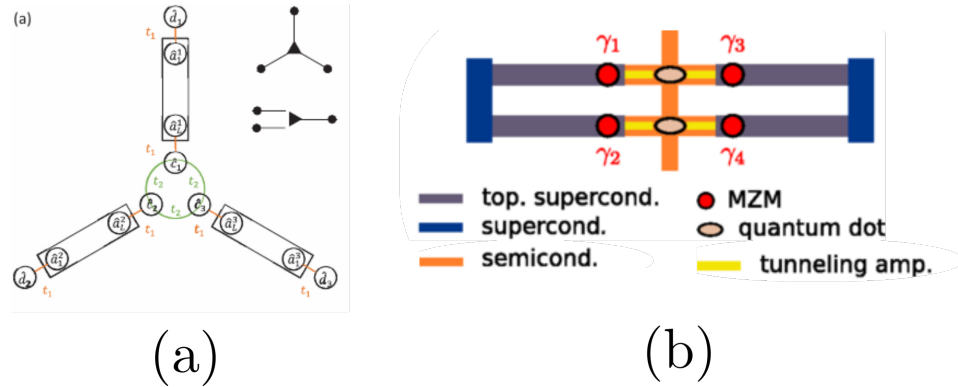


Figure 3.8: a) Braiding proposal b) Basic architecture with four Majorana Zero Modes in a scalable quantum computer.

Source: Adapted from (a) [30] (b) [31].

Nonetheless, the future for this area is still very promising. Recent experiments have documented the observation of Majorana signatures in Majorana-QD devices [13] and Andreev molecules in topological superconductors attached to double quantum dots [32]. The next steps are clearly directed to achieve Majorana manipulation.

3.2.1 Why double quantum dots?

The simplest case where Majorana manipulation is possible is in a double quantum dot (DQD). Tunneling Majorana modes in these basic structures have inspired theoretical studies [33, 34] and experimental setups confirming the observations of Andreev molecules [32]. Even though quantum tunneling of a MZM into a double dot shows several possibilities for manipulation of MZM, there is still no complete analysis of the transitions of the Majorana signatures between the QDs in this model.

In this thesis we fill this gap by performing a transport study of a DQD attached to a MZM and a metallic lead. The simplicity of this model allows us to explore analytically different configurations of QD's from symmetric and linear couplings to T-junctions . We considered both non-interacting and interacting regimes, observing major agreement between both approaches about the location of the Majorana signature. While the non-interacting regime is suitable to obtain exact expressions for the Green function, the interacting case shows how the Majorana signature co-exists with strongly correlated phenomena such as the Kondo effect and RKKY interactions [35–37].

3.3 Overview

This thesis is integrated by 4-major chapters:

- In chapter 4, we will take a review to the basis of quantum transport in single electron transistors, the Anderson model and the emergence of the Kondo effect in quantum dots.
- In ?? we provide a description of the methods that we will use to study the Double Quantum Dot-Majorana system. To study non-interacting systems we will use the Zubarev's ballistic transport[38] which is optimized through the Graph-Gauss-Jordan elimination algorithm define in ???. For non-interacting systems we use Wilson's Numerical Renormalization Group (NRG) technique [39]. We will probe our methods in a double quantum dot attached to a magnetic field. Hence, background information about double quantum dots systems will be presented in this chapter.
- In chapter 5 We will probe our methods in the QD-Majorana system, confirming the results of previous papers [26, 40] .
- The ?? contains our major contributions to this area. Using the methods from ?? and the previous acquired experience with the double quantum dot and the QD-Majorana model ,

3.3. Overview

we study in a double quantum dot attached to a Majorana zero mode and a metallic lead. We will characterize in this simple model the transitions of the Majorana signature for distinct configurations of the dots. The final results are now part of a paper that we hope to submit for publication in the following months.

Chapter 4

Preliminaries

In this chapter we will give a brief description about transport processes in quantum dots (QDs). This will lead us to talk discuss the Anderson model and the Kondo effect, which are key ingredients in the objective of this project .

4.1 Transport in Quantum Dots (QDs)

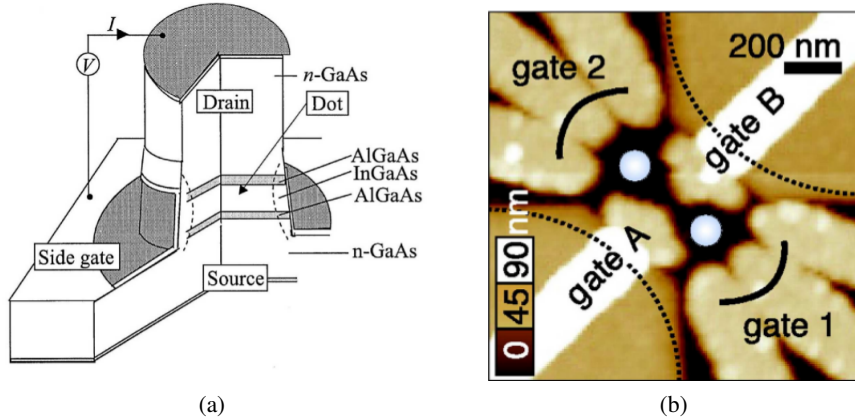


Figure 4.1: a) Vertical quantum dot. b) Atomic force microscopy picture of two coupled lateral QDs (bright central circles). Gates 1 and 2 act as drain and source voltage. A negative voltage is applied at gates A,B to allow the formation of the droplets inside the free space in the 2D electron gas.

Source: [41]

Quantum mechanical effects are visible when the system size is of the order of the de Broglie wavelength [42, (1.1)]

$$\lambda_f = \frac{h}{\sqrt{3m_{\text{eff}}k_B T}}$$

where m_{eff} is the electron effective mass in the crystal. Since m_{eff} can be much smaller than the free electron mass in some semiconducting materials, size quantization effects can be observed at system of sizes $\sim 100\text{nm}$ [43, 2.1]. A 0D quantum system is a device confined in the three

4.1. Transport in Quantum Dots (QDs)

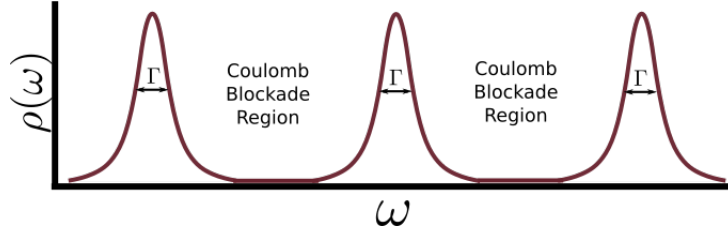


Figure 4.2: Pictorial representation of the Density of States of a QD. The gate potential V_G can be tuned to change the fermi energy of the dot.

Source: By the author

spacial dimensions up to this length-scale. This type of devices receive the name of quantum dots (QD).

Nowadays, QDs can be manufactured with different substracts, geometries and orientations [42]. They can be merged in structures like double quantum dots (4.1a) or can even be built out vertical to the base 2D-electron gas (4.1b). The precise experimental control over these devices allows to design atom-like structures with controllable energy levels. This has important applications on laser physics and in the implementation of single electron transistors.

Usually quantum dots have 3-main gates. Two of them are the Drain V_D and source V_S voltages used to control the electric gradient through the QD. The third one is the gate voltage V_G which allows to control with high precision the number of electrons inside the dot.

Ideally, the energy spectrum of a QD is a discrete set of energy levels resembling the spectrum of an atom. When the QD is connected to metallic leads these energy levels hybridized with respect to a broadening parameter Γ which increases as the square of the source-drain voltage V_{SD}

$$\Gamma \propto \pi \|V_{SD}\|^2 \quad (4.1)$$

in a flat band approximation. This broadening is depicted in Figure 4.2. Ideally, $\Gamma \ll \Delta E$ is smaller enough such that the energy levels do not overlap each other.

It is possible to execute transport measurements through a QD attached to two leads, source and drain (See 4.3a) . Each lead will have a characteristic gate voltage V_S (Left lead) and V_D (Right lead). An electron can pass from the source to the drain if there is an energy level in the middle of the two voltages, just as in 4.3a. If this condition is not satisfied, the dot enters into a coulomb blockade region without electron transport between both leads as can be observed in 4.3b. Inside the coulomb blockade regions described (black diamonds) the number of electrons is constant. When increasing V_G a single electron enters into the dot each time the system makes a transition between blockade regions. Since all of these effects can be controlled precisely with the gate voltage, the system described is indeed a single electron transistor (SET).

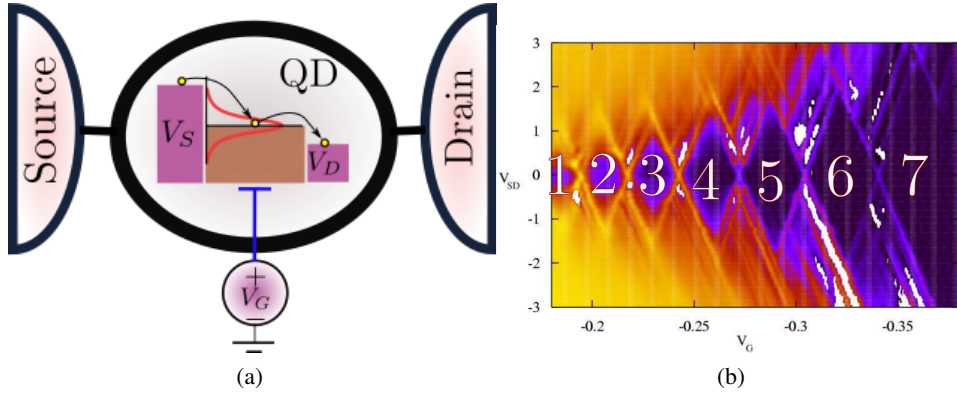


Figure 4.3: a) Representation of transport through QD. The red curve represents the hybridized energy level. The gate voltage tunes this level. In the case represented, the energy level is in the middle of the drain and source voltages allowing transport between the leads. b) Charging diagram of a quantum dot. Differential conductance dependence over the gate voltage V_G and the source-drain voltage ($V_{SD} = V_S - V_D$). Coulomb blockade occurs at the diamond-shaped regions with zero conductance. At these regions the number of electrons is constant and increases 1 by 1 when the gate voltage is scaled up.

Source: a) By the Author , b) Adapted from [43]

4.2 The Anderson Model

The Anderson model is used to describe quantum impurity systems where Coulomb repulsions and strongly correlated phenomena are dominant [44]. A quantum dot attached to a metallic lead is basically an artificial impurity that can be experimentally designed, modified and manipulated. Hence QDs are the perfect type of structure to probe the of the physics behind Anderson's ideas.

Due to the small confinement space inside these dots, the coulomb repulsion is relevant. However, it is usually impossible to provide a complete analytical description of these kind of systems due to the high correlations generated by this factor. Instead, we can obtain an overall description of the transport through the impurity by neglecting this coulomb repulsion. This will allow us to obtain some analytic intuition of the models before adventuring with long-lasting numerical simulations of interacting models. During this thesis, we will consider these two regimes as follows

- **Non-interacting systems:** Coulomb repulsion is not relevant . In this case, spin- \uparrow and spin- \downarrow channels are independent which simplifies many of the procedures. They can be described analytically through the ballistic transport approach.
- **Interacting systems:** The coulomb repulsion is relevant. The repulsion factor will be defined by the factor U which will take a fix value during the entire project. In this case,

4.2. The Anderson Model

spin- \uparrow and spin- \downarrow channels are not independent since the coulomb repulsion limits the number of particles inside each dot. We will use the Numerical Renormalization Group to treat this case. The intuition acquired from non-interacting systems will help us to select the input parameters of the algorithm.

To build the Anderson model first consider that we have a QD (impurity) coupled to the conduction band of a metallic lead. We will define a coulomb repulsion factor U which will be set to 0 if the system is non-interacting. Using the Hunds rules we know that the energy levels inside the dot should be filled from lower to higher energies with two electrons with different spin at each state. Each pair of electrons will interact magnetically and electrically. In addition, there is an energy term associated to each electron and a Zeeman splitting factor in case a \hat{z} -directed magnetic field B is placed. Considering these interactions we can obtain a very general expression in second quantization for the QD Hamiltonian of the form [43, (3.2)]

$$H_d = \sum_{i\sigma} \varepsilon_{di} d_{i\sigma}^\dagger d_{i\sigma} + \sum_i U_i \hat{n}_{i\uparrow} \hat{n}_{i\downarrow} + \sum_{\sigma\sigma', i \neq j} U_{ij} \hat{n}_{i\sigma} \hat{n}_{j\sigma'} - \mu_B g B \sum_i S_i^z + J \sum_{i \neq j} \mathbf{S}_i \cdot \mathbf{S}_j.$$

Where $\sigma \in \{\uparrow, \downarrow\}$, $d_{i\sigma}^\dagger$ ($d_{i\sigma}$) is the dot creation(annihilation) operator, $\hat{n}_{i\sigma} := d_{i\sigma}^\dagger d_{i\sigma}$ is the particle number, \mathbf{S}_i is the spin-vector, ε_{di} is the energy of the i^{th} -level in the dot, U_i is the coulomb repulsion between electrons in the same energy level i , U_{ij} is the coulomb interaction between electrons in different levels (And therefore smaller than U_i), B is an applied magnetic field in the \hat{z} -direction and J is the term representing the Zeeman splitting.

At low temperatures, the quantum interactions occur only with the level closest to the Fermi energy. This allows us to make the single-level approximation, neglecting the other energy levels. This assumption reduces the complexity of the dot Hamiltonian to

$$H_d = \sum_{\sigma} \varepsilon_d d_{\sigma}^\dagger d_{\sigma} + U \hat{n}_{\uparrow} \hat{n}_{\downarrow} - \mu_B g B S^z. \quad (4.2)$$

Besides to the dot Hamiltonian, we need to consider the energy of the electrons in the lead H_{lead} and the dot-lead interaction H_{int} . We can model the conduction band of the lead as a 2D electron gas with the following Bloch Hamiltonian

$$H_{\text{lead}} = \sum_{\mathbf{k}\sigma l} \varepsilon_{\mathbf{k}l} c_{\mathbf{k}\sigma l}^\dagger c_{\mathbf{k}\sigma l}. \quad (4.3)$$

where \mathbf{k} represents the possible crystal momentums in the leads, $l \in \{S, D\}$, $c_{\mathbf{k}\sigma l}^\dagger$ ($c_{\mathbf{k}\sigma l}$) creates(annihilates) an electron with momentum \mathbf{k} and spin σ in the lead l , $\varepsilon_{\mathbf{k}l}$ is the energy of the electron in the leads.

The interaction between the dot and the leads is then given by

$$H_{\text{int}} = \sum_{\mathbf{k}\sigma l} V_{\mathbf{k}l} c_{\mathbf{k}\sigma l}^\dagger d_{\sigma} + V_{\mathbf{k}l}^* d_{\sigma}^\dagger c_{\mathbf{k}\sigma l}, \quad (4.4)$$

4.3. The Kondo Effect

where $V_{\mathbf{k}l}$ is a hopping exchange term between the leads and the QD.

The sum of all of these three interactions is receives the name of Anderson Model.

$$\begin{aligned} H &= H_d + H_{lead} + H_{int} \\ &= \sum_{\sigma} \varepsilon_d d_{\sigma}^{\dagger} d_{\sigma} + U \hat{n}_{\uparrow} \hat{n}_{\downarrow} - \mu_B g B S^z + \sum_{\mathbf{k}\sigma l} \varepsilon_{\mathbf{k}l} c_{\mathbf{k}\sigma l}^{\dagger} c_{\mathbf{k}\sigma l} + \sum_{\mathbf{k}\sigma l} V_{\mathbf{k}l} c_{\mathbf{k}\sigma l}^{\dagger} d_{\sigma} + V_{\mathbf{k}l}^* d_{\sigma}^{\dagger} c_{\mathbf{k}\sigma l}. \end{aligned} \quad (4.5)$$

For this project, we will make two extra changes to the Anderson model. Using the anti-commutation properties of the fermion operators

$$\{d_{\sigma}^{\dagger}, d_{\sigma'}\} = \delta_{\sigma\sigma'}, \quad \{d_{\sigma}^{\dagger}, d_{\sigma'}^{\dagger}\} = \{d_{\sigma}, d_{\sigma'}\} = 0$$

we get

$$\begin{aligned} (d_{\uparrow}^{\dagger} d_{\uparrow} + d_{\downarrow}^{\dagger} d_{\downarrow} - 1)^2 &= \sum_{\sigma} (d_{\sigma}^{\dagger} d_{\sigma})^2 - 2 \sum_{\sigma} d_{\sigma}^{\dagger} d_{\sigma} + 2 d_{\uparrow}^{\dagger} d_{\uparrow} d_{\downarrow}^{\dagger} d_{\downarrow} - 1 \\ &= 2 d_{\uparrow}^{\dagger} d_{\uparrow} d_{\downarrow}^{\dagger} d_{\downarrow} - \sum_{\sigma} d_{\sigma}^{\dagger} d_{\sigma} - 1. \end{aligned}$$

Replacing this in (4.2) we obtain a nice spin-symmetric form of the dot hamiltonian

$$\left(\varepsilon_d + \frac{U}{2} \right) d_{\sigma}^{\dagger} d_{\sigma} + \frac{U}{2} (d_{\sigma}^{\dagger} d_{\sigma} - 1)^2 - \mu_B g B S^z. \quad (4.6)$$

In addition, it is possible to do a linear transform to the lead operators

$$\frac{1}{\sqrt{V_S^2 + V_R^2}} \begin{bmatrix} V_S & V_R \\ -V_R & V_S \end{bmatrix} \begin{bmatrix} c_{\mathbf{k}\sigma S} \\ c_{\mathbf{k}\sigma D} \end{bmatrix} = \begin{bmatrix} c_{\mathbf{k}\sigma+} \\ c_{\mathbf{k}\sigma-} \end{bmatrix} \quad (4.7)$$

After the transformation the operator will be decoupled from the dot hamiltonian $c_{\mathbf{k}\sigma-}$. This implies that we can suppose that the **dot is coupled wit just one lead**. During the rest of the thesis we will maintain this convention.

4.3 The Kondo Effect

The Kondo effect is one of the biggest condensed matter problems in the 20th century. There was an uncountable number of experimental and theoretical physicist that contributed to this problem . The most reknown are probably the physicists Jacques Friedel, Jun Kondo and the two nobel prizes Philip Anderson and Kenneth Wilson [47].

The history of the Kondo effect began in the early 1930s. By that time it was known that the resistivity of a metal is regulated by different scattering interactions against lattice phonon vibrations $\rho_{phonon} \sim T^5$, other electrons $\sim T^2$ and static impurities, which is temperature independent. The form of these contribution clearly implies that the resistivity should decay

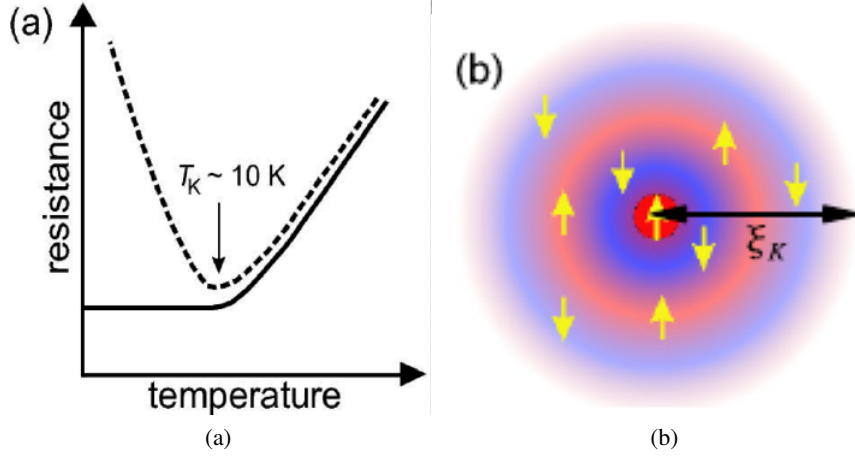


Figure 4.4: a) Resistivity minimum near the Kondo temperature T_k . b) Kondo cloud formed by a singlet grouped around the impurity divided in spin- \uparrow ,spin- \downarrow regions.

Source: a) [45], b) [46]

uniformly with a decreasing temperature. Nevertheless, some groundbreaking experiments revealed the observation of a resistance minimum in some metals at temperatures lower than 10K [45] (See 4.4a).

This phenomenon intrigued the scientific community for the following decades until the year 1964 when the physicist Jun Kondo gave the first convincing solution to this puzzle. Kondo attributed the phenomenon to the scattering of the electrons due to the spin-interaction with a small concentration of magnetic impurities in the metal. To describe it he proposed the following interaction Hamiltonian

$$H_K = 2J\hat{\mathbf{S}} \cdot \hat{\mathbf{s}} \quad (4.8)$$

$$= J(2S_zs_z + S_+s_- + S_-s_+) \quad (4.9)$$

with $S_{\pm} = S_x \pm iS_y$. The hamiltonian H_K which is better known as the Kondo s-d model describes the spin interaction between the spin of the impurity $\hat{\mathbf{S}}$ and the spin of the particles in the metal $\hat{\mathbf{s}}$.

Kondo took H_K as a perturbation of the electron gas inside metallic lead, with J the perturbation parameter. While the first order led to no important contribution, Kondo was able to obtain on second order perturbation theory a logarithmic correction on the temperature in the resistivity of the form

$$\rho_{imp} \propto \ln \frac{T_K}{T}, \quad (4.10)$$

4.3. The Kondo Effect

where T_K received the name of Kondo temperature. Summing up this term to the other resistivity contributions we obtain the full expression

$$\rho_{metal}(T) = \rho_{imp} + a_e T^2 + b_{Phonon} T^5 + c_m \ln \frac{T_K}{T}. \quad (4.11)$$

Note that when $T < T_K$ the term $\ln \frac{T_K}{T}$ increases. Eventually, it compensates the decaying resistivity which finally explained the resistance minimum.

Although Kondo's explanation was initially very successful it also presented a troublesome outcome. The logarithmic term introduced by Kondo diverges when the temperature approximates to 0, hence proving to be inefficient at temperatures well below T_K . Going to the following orders in perturbation theory also led to divergent resistivities which led the to explore non-perturbative approaches to solve the Kondo effect.

On the other hand, Anderson had already created his famous impurity model. One of his main contributions was the inclusion of the Hubbard term to represent the Coulomb interaction inside the dot, which proofed to be fundamental to understand the Kondo effect. Years later, Kenneth Wilson was able to effectively diagonalize the Anderson model using a numerical method that combines ideas from scalability and the renormalization group.

Wilson's explanation solved the Kondo problem almost completely. It turned out that at very low temperatures, the impurity entangles with the low-energy electrons forming a strongly correlated many-body singlet. This singlet surrounds the impurity in a structure formed by alternating regions of spin- \uparrow and spin- \downarrow particles called the Kondo cloud (See Figure 4.4b). This Kondo cloud is predicted to have an astonishing correlation length between $0.1\mu m$ to $10\mu m$. This is a huge radius if we think that the impurity(or QD) can have a radius bellow $1nm$. The Kondo effect, is produces when the conduction electrons scatter with the Kondo cloud, which increases the resistivity of the material.

4.3.1 Kondo Effect in QDs

The problem of magnetic impurities in metals can be treated using the Anderson model in a similar form as the transport in quantum dots. Hence, it is not a surprise that the Kondo Effect could also occur these systems. In 1998 the technological advances allowed the observation of the Kondo effect for the first time in a single electro transistor [49]. When an odd number of electrons is in the QD the last level bellow the Fermi energy is half-occupied and hence the dot can be considered as a magnetic impurity. The unlocalized electrons in the reservoirs then interact with this localized electron. Spin-exchange can occur as it happened with magnetic impurities in metals. At low temperatures, this magnetic interaction gives rise to strong quantum correlations that favor the formation of a singlet state between the localized electron and the electrons in the leads. As a result, the zero-bias density of states is increased producing a zero-bias conductance peak Figure 4.5(b).

4.3. The Kondo Effect

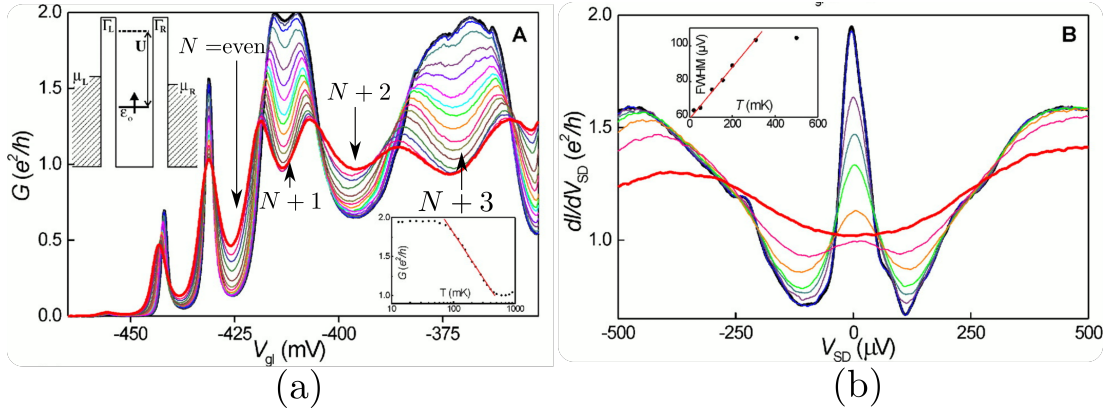


Figure 4.5: Observation of the Kondo effect in a single electron transistor. Color scale temperatures from 15mK (Black) to 800mK(Red) a) Dependence of the zero bias conductance over the gate voltage. A plato in the conductance peak appears in the odd particle regimes. b) Dependence of the conductance over the gate source drain voltage inside an odd electron regime. A zero bias conductance peak (ZBCP) of height $\frac{2e^2}{h}$ is observed. This is the Kondo signature.

Source: [48]

Note that the physical implications of the Kondo effect between the case of magnetic impurities in metals and transport through QD are different. The reason for this are the dimensions of the system. While the scattering at 3D systems against magnetic impurities is an obstacle to conduction electrons, the scattering in 0D systems enhances the conductivity of the QD since there is only one scattering direction.

As we previously discussed, transport in quantum dots can occur only if there is a state in the middle of the drain and source voltage. The Kondo effect creates a zero bias peak that is present whenever the dot has odd electrons . This explains the zero-bias plateaus observed in Figure 4.5(a). We may think that the new singlet state at the Fermi energy is creating a "channel" that allows quantum transport between both sides of the dot.

Chapter 5

Coupling a QD with a Majorana chain

Liu and Baranger were the first to propose in 2011 the possibility of using QDs in the pursuit of Majorana fermions . When a QD is attached to the end of a Majorana chain in the topological phase, the Majorana Zero Mode at the end of the chain leaks inside the QD [27] producing a zero-bias conductance peak of half a quanta $\frac{e^2}{2h}$ through the dot. This method of detecting Majorana signatures presents the following advantages:

1. The qubit information is not completely destroyed, in contrast to other detection methods such as tunneling spectroscopy.
2. If performed under the Kondo temperature T_k it allows the possibility of observing the MZM co-existing with the Kondo peak, [1, 22, 29] .
3. Today's precise experimental control over the QD parameters allows the manipulation of MZMs inside multi-dot systems, which offers new possibilities to design of quantum architectures with Majorana chains.[31, 50]

In this project we will exploit the second and the third properties to manipulate MZMs in double quantum dot systems in the Kondo regime. But before going through that model, it is necessary to understand the single dot-Majorana coupling.

5.1 Model

In this section we will recreate the results of Liu and Baranger using the methods developed in ?? . This will also allow us to probe our methods in a system with Majorana zero modes.

The Hamiltonian for Majorana-QD-lead hybrid system (See Figure 5.1) is given by

$$H = H_{QD-Lead} + H_{M-QD} + H_M. \quad (5.1)$$

Where $H_{QD-Lead}$ is the Hamiltonian for the non-interacting Anderson model (4.5), H_M is the Hamiltonian of the Majorana chain and H_{M-QD} represents the coupling between the QD and the Majorana Fermion at the boundary.

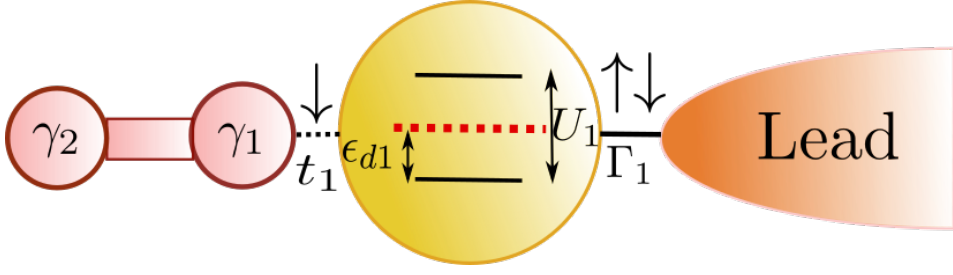


Figure 5.1: Model for the QD-Majorana system. Solid lines: Hopping interactions: V_1 couplings of QD1 . Dashed lines: Majorana spin- \downarrow effective couplings (5.2) t_1 . The atomic energy levels appear inside each QD ϵ_1 are tuned by the gate voltages. The coulomb interaction is represented by U_1 separates two energy levels. The red dashed horizontal lines represent the Fermi level.

Now, the real question is how to define the coupling between the QD and the Majorana fermion. In fact, there are many ways to represent this interaction. One alternative is to replace in H_M with the entire Kitaev chain hamiltonian (3.1) (or even with the Majorana chain (3.18)) and then pick H_{M-QD} as a simple coupling between the QD and the first site of the chain [27]. A simpler approach is to define an effective coupling with the Majorana operator at the edge of the Majorana chain. Since the Kitaev chain is spin-less, we choose to couple the Majorana to the spin- \downarrow channel of the QD ⁴. Therefore, the Majorana fermion should be the superposition of the creation and annihilation operators of a spin \downarrow particle f_\downarrow :

$$\gamma_1 := \frac{1}{\sqrt{2}} (f_\downarrow^\dagger + f_\downarrow), \gamma_2 := \frac{1}{\sqrt{2}} (f_\downarrow^\dagger - f_\downarrow).$$

This makes possible to define an effective coupling between the Majorana Mode and the dot by attaching γ_1 with the spin- \downarrow channel in the QD

$$H_{M-QD} = t_1 (d_\downarrow^\dagger \gamma_1 + \gamma_1 d_\downarrow) \quad (5.2)$$

Then the coupling with the chain is given by

$$\begin{aligned} H_M &= \epsilon_m f_\downarrow^\dagger f_\downarrow \\ H_{M-QD} &= \frac{t_1}{\sqrt{2}} d_{1\downarrow}^\dagger f_\downarrow + \frac{t_1^*}{\sqrt{2}} f_\downarrow^\dagger d_{1\downarrow} + \frac{t_1}{\sqrt{2}} d_{1\downarrow}^\dagger f_\downarrow^\dagger + \frac{t_1^*}{\sqrt{2}} f_\downarrow d_{1\downarrow} \end{aligned}$$

Finally we obtain the following hamiltonian

⁴An appropriate justification of this fact can be found in [1]

$$H = \sum_{k,\sigma} \left(\epsilon_1 + \frac{U_1}{2} \right) d_{1\sigma}^\dagger d_{1\sigma} + \frac{U}{2} (d_{1\sigma}^\dagger d_{1\sigma} - 1)^2 + t_1 (d_{1\downarrow}^\dagger \gamma_1 + \gamma_1 d_{1\downarrow}) + V d_{1\sigma}^\dagger c_{k\sigma} + V^* c_{k\sigma}^\dagger d_{1\sigma} + \epsilon_m f_\downarrow^\dagger f_\downarrow. \quad (5.3)$$

The fidelity of this effective model has been discussed by Ruiz-Tijerina et al. [1] concluding that this model reproduces the same results than coupling a Kitaev chain model in the topological phase to a QD. (This statement is true even for more realistic models of the TS including Rashba spin-orbit interactions and a Zeeman field [1]).

5.2 Non-interacting QD coupled to Majorana chain

In the non-interacting case we can use the ballistic transport equations from ?? .The green functions are then determined by the following set of linear equations.

$$(\omega - \epsilon_M) G_{f_\downarrow, d_{1\downarrow}^\dagger}(\omega) = (\omega + \epsilon_M) G_{f_\downarrow^\dagger, d_{1\downarrow}^\dagger}(\omega) = \frac{t_1^*}{\sqrt{2}} (G_{d_{1\downarrow}, d_{1\downarrow}^\dagger}(\omega) - G_{d_{1\downarrow}^\dagger, d_{1\downarrow}^\dagger}(\omega)) \quad (5.4)$$

$$(\omega - \epsilon_1) G_{d_{1\downarrow}, d_{1\downarrow}^\dagger}(\omega) = 1 + \frac{t_1}{\sqrt{2}} t_1 G_{f_\downarrow, d_{1\downarrow}^\dagger}(\omega) + \frac{t_1}{\sqrt{2}} t_1 G_{f_\downarrow^\dagger, d_{1\downarrow}^\dagger}(\omega) + V_1 \sum_{\mathbf{k}} G_{c_{\mathbf{k}\downarrow}, d_{1\downarrow}^\dagger}(\omega) \quad (5.5)$$

$$(\omega - \epsilon_{\mathbf{k}}) G_{c_{\mathbf{k}}, d_{1\downarrow}^\dagger}(\omega) = V_1^* G_{d_{1\downarrow}, d_{1\downarrow}^\dagger}(\omega) \quad (5.6)$$

$$(\omega + \epsilon_1) G_{d_{1\downarrow}^\dagger, d_{1\downarrow}^\dagger}(\omega) = -\frac{t_1}{\sqrt{2}} G_{f_\downarrow, d_{1\downarrow}^\dagger}(\omega) - \frac{t_1}{\sqrt{2}} G_{f_\downarrow^\dagger, d_{1\downarrow}^\dagger}(\omega) - V_1^* \sum_{\mathbf{k}} G_{c_{\mathbf{k}\downarrow}^\dagger, d_{1\downarrow}^\dagger}(\omega) \quad (5.7)$$

$$(\omega + \epsilon_{\mathbf{k}}) G_{c_{\mathbf{k}}^\dagger, d_{1\downarrow}^\dagger}(\omega) = -V_1^* G_{d_{1\downarrow}, d_{1\downarrow}^\dagger}(\omega) \quad (5.8)$$

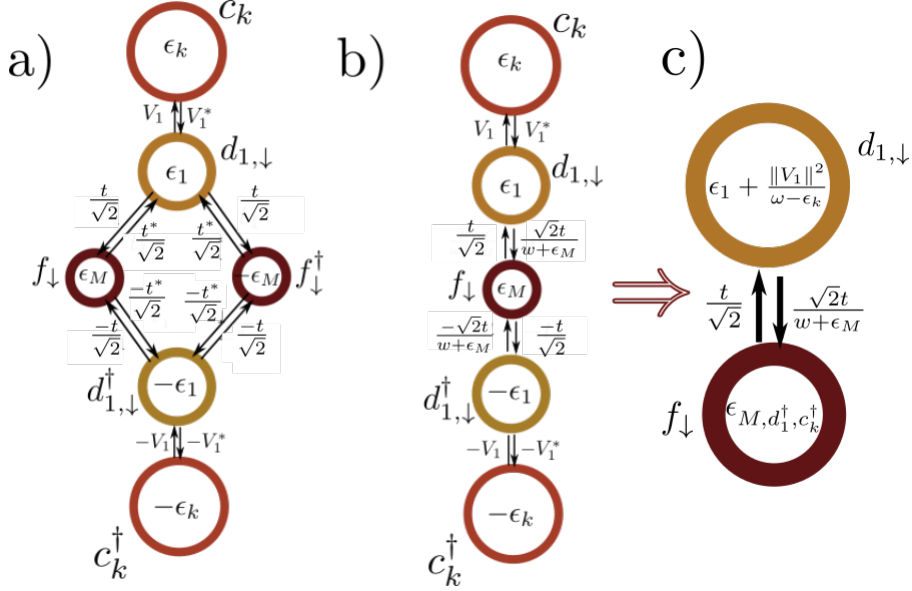
The graph representing these green functions is represented in Figure 5.2 a) (Look ?? for details). However using that $(\omega - \epsilon_M) G_{f_\downarrow, d_{1\downarrow}^\dagger}(\omega) = (\omega + \epsilon_M) G_{f_\downarrow^\dagger, d_{1\downarrow}^\dagger}(\omega)$ we can take $G_{f_\downarrow^\dagger, d_{1\downarrow}^\dagger}(\omega)$ out of the equations. After eliminating this term 5.5 becomes

$$(\omega - \epsilon_1) G_{d_{1\downarrow}, d_{1\downarrow}^\dagger}(\omega) = 1 + \frac{t_1}{\sqrt{2}} \left(1 + \frac{\omega - \epsilon_M}{\omega + \epsilon_M} \right) G_{f_\downarrow, d_{1\downarrow}^\dagger}(\omega) + V_1 \sum_{\mathbf{k}} G_{c_{\mathbf{k}\downarrow}, d_{1\downarrow}^\dagger}(\omega) \quad (5.9)$$

$$= 1 + \frac{\sqrt{2}t_1}{\omega + \epsilon_M} G_{f_\downarrow, d_{1\downarrow}^\dagger}(\omega) + V_1 \sum_{\mathbf{k}} G_{c_{\mathbf{k}\downarrow}, d_{1\downarrow}^\dagger}(\omega) \quad (5.10)$$

Similarly,

$$(\omega + \epsilon_1) G_{d_{1\downarrow}^\dagger, d_{1\downarrow}^\dagger}(\omega) = -\frac{\sqrt{2}t_1}{\omega + \epsilon_M} G_{f_\downarrow, d_{1\downarrow}^\dagger}(\omega) - V_1^* \sum_{\mathbf{k}} G_{c_{\mathbf{k}\downarrow}^\dagger, d_{1\downarrow}^\dagger}(\omega) \quad (5.11)$$


 Figure 5.2: Graph \mathcal{G}_M representing the transport equations. Source: By the author

With these new equations we obtain new associated graph is in Figure 5.2 b) . Using the graph algorithm from ?? we proceed to pop out vertexes c_k , c_k^\dagger and d_1^\dagger in that order. The result is the graph in figure Figure 5.2.c) with

$$\epsilon_{M,d_1^\dagger,c^\dagger} = \epsilon_M + \frac{\omega}{\omega + \epsilon_M} \frac{\|t\|^2}{\omega + \epsilon_1 + \sum_{\mathbf{k}} \frac{V_1 V_1^*}{\omega + \epsilon_{\mathbf{k}}}}. \quad (5.12)$$

We finally pop out f_d to obtain

$$G_{d_{1,\downarrow},d_{1,\downarrow}^\dagger}(\omega) = \left[\omega - \epsilon_1 - \sum_{\mathbf{k}} \frac{V_1 V_1^*}{\omega - \epsilon_1} - \frac{\omega}{\omega + \epsilon_M} \frac{\|t\|^2}{\omega - \epsilon_{M,d_1^\dagger,c^\dagger}} \right]^{-1}. \quad (5.13)$$

This is the Green function we have been looking for. After a few algebraic operations it is possible to show that this result is equivalent to the first computation done by Liu and Baranger in the paper [26].

To compute the DOS we need to replace $\sum_{\mathbf{k}} \frac{V_1 V_1^*}{\omega - \epsilon_{\mathbf{k}}} = -i\Gamma_1$ as we already did in ?? . Note that these computations are only for the spin- \downarrow channel. The spin- \uparrow channel is even simpler since this channel is not coupled to the Majorana mode by convention. Hence it corresponds to the case of a single quantum dot coupled to a Lead. The results for the DOS can be observed in Figure 5.3. Each figure has an inset showing the model in the Majorana representation. The small blue and red balls are Majorana fermions just as the ones in figure Figure 3.2. The Majorana at the edge of the chain is represented by the isolated red ball connected to the QD (Figure 5.3a). The other

5.2. Non-interacting QD coupled to Majorana chain

isolated blue ball in Figure 5.3c represents the Majorana at the other edge which is connected to the sphere by the parameter ε .

- **Figure 5.3.(a),(b):** The spin- \uparrow DOS shows the result of coupling the QD with the lead and without Majorana fermions. When the parameter t is increased, the Majorana fermion is couple to the spin- \downarrow which causes the dispersion of the DOS. The most relevant signature is the robust height of 0.5 in the DOS that is observed in the central peak for all $t > 0$. This mid-height DOS is responsible for the decay of half a quanta in the conductivity of the QD.

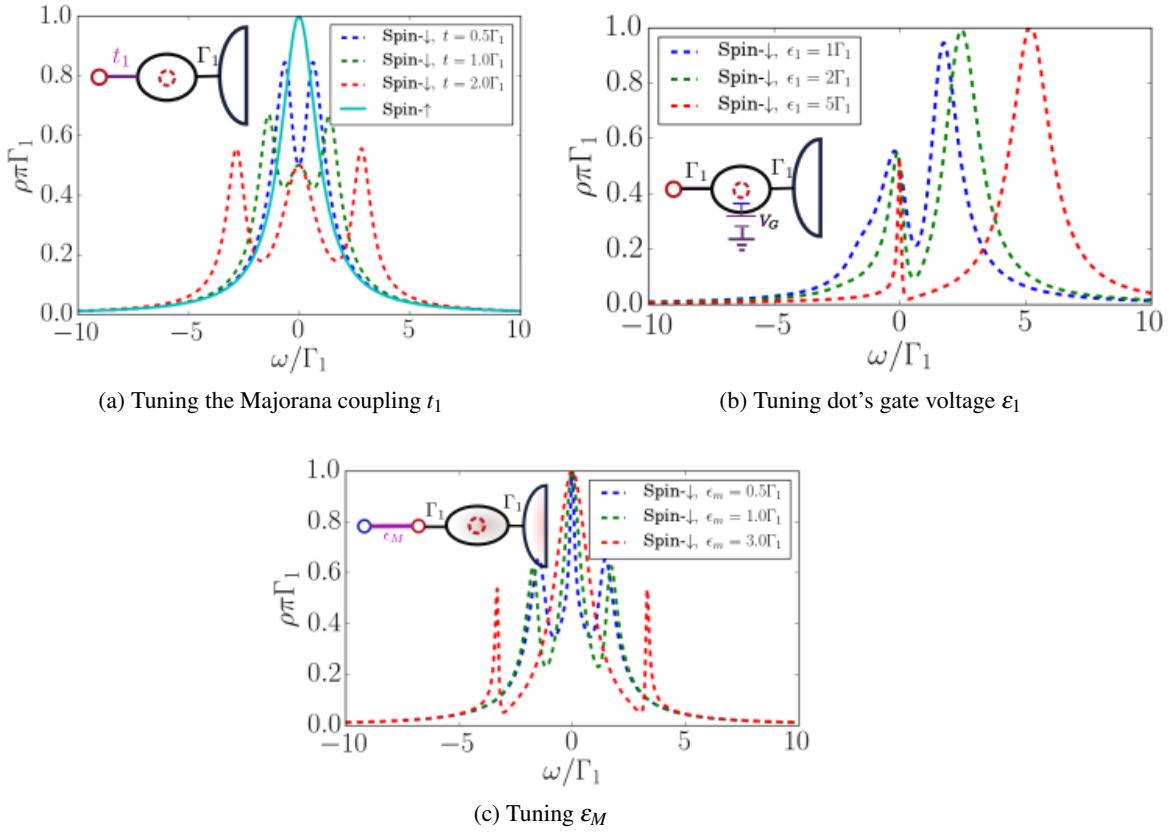


Figure 5.3: Density of states for a Majorana coupled to a QD under the tuning of different parameter. The tuning parameter is drawn in purple line in the inset model.

Source: *By the author*

- **Figure 5.3.(c),(d):** This time a gate voltage is induced in the dot which breaks PHS. However the robust 0.5-height Majorana signature prevails in the dot even at very high gate voltages where the dot is expected to be empty.

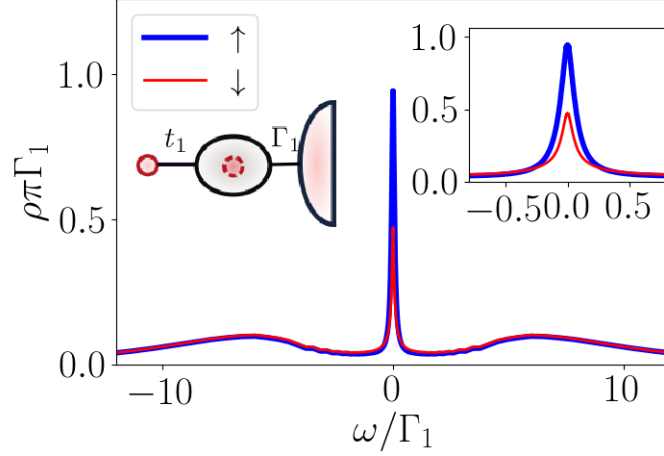


Figure 5.4: DOS at $t_1 = \Gamma_1$ at the PHS-point. Insets: Left: QD-Majorana model. Right: Low energy DOS.

Source: By the author.

- **Figure 5.3.(e),(f):** The term ε_M couples both Majoranas at the edges of the chain. The strength of this parameter decays exponentially with the length of the Majorana chain so that it is often neglected . Here we observe the consequences of including this parameter in the model. The spin- \downarrow DOS emulates the spin- \uparrow DOS for energies $\omega < \varepsilon_M$. This clearly destroys the Majorana zero mode.

5.3 Kondo-Majorana physics

In interacting quantum dots the Kondo effect is visible at low temperatures even when the QD is attached to a Majorana chain, which allows the study Kondo-Majorana physics. To observe this , we used the NRG code with a fixed Coulomb repulsion of $U = 17.6\Gamma_1$ just as in section ???. Then, particle-hole equilibrium is achieved when $(\varepsilon_1 + \frac{U_1}{2}) \hat{n}_1\sigma$. Any tuning of the dots gate voltage must be understood as a displacement $\Delta\varepsilon_1$ from this equilibrium point.

Figure 5.4 shows the PHS case for a Majorana coupling $t_1 = \Gamma_1$. The two small wide peaks at the borders of the plot are the coulomb states. In the right inset of the figure, we observe the low-temperature regime inside the gap. There, two zero modes can be appreciated. While the spin- \uparrow DOS is the same Kondo peak from Figure ???, the spin- \downarrow DOS reveals a Majorana zero mode of half the amplitude of the Kondo peak $(\frac{0.5}{\pi\Gamma_1})$. This Majorana signature resembles the one in Figure 5.3a.

It is possible to separate Kondo and Majorana physics by inducing a gate voltage in the dot. As observed in Figure 5.5(a), the gate voltage detunes the Kondo peak from the Fermi

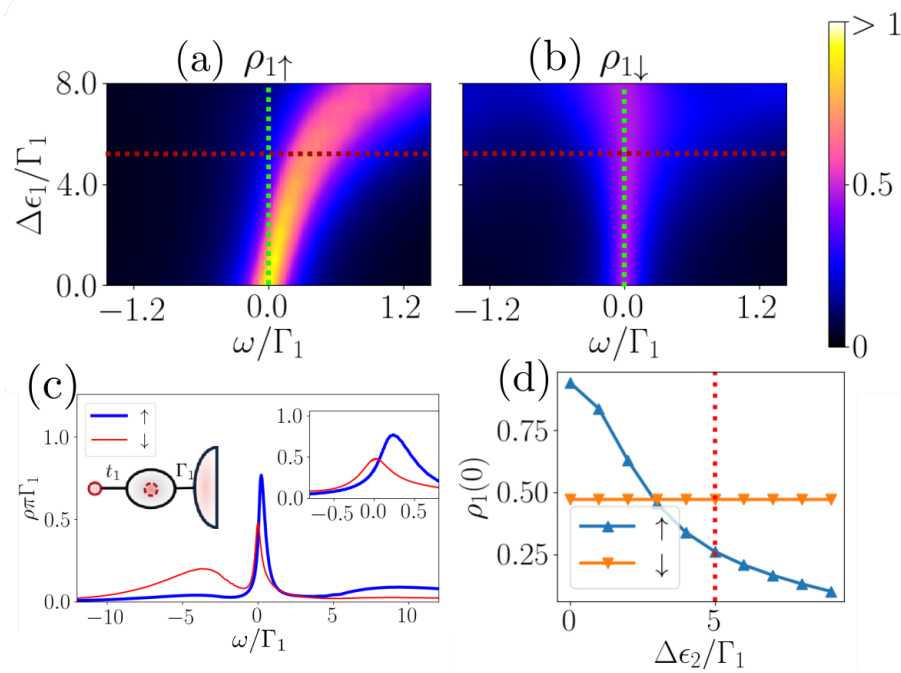


Figure 5.5: (a)&(b): Dependance of the DOS over the gate voltage $\Delta\epsilon_1$ at $t_1 = \Gamma_1$. (a) Spin- \uparrow (b) Spin- \downarrow . (c) DOS at the red-dashed horizontal cut in (a)&(b). Insets: Left: QD-Majorana model. Right: Low energy DOS. (d) DOS at the Green-dashed vertical cut in (a)&(b).

Source: By the author.

energy. Instead, the MZM in Figure 5.5(b) remains at the same position. At $\Delta\epsilon_1 = 5\Gamma_1$ we can already observe a decaying Kondo peak next to the robust Majorana signature of height $\frac{0.5}{\pi\Gamma_1}$ (Figure 5.5(c)). This is more clear in Figure 5.5(d) where the spin- \uparrow DOS decays with $\Delta\epsilon_1$ while the spin- \downarrow DOS is stable, even at $\Delta\epsilon_1 \sim \frac{U}{2} = 8.6$ where the dot is supposed to be empty.

This interesting result was already pointed out by Ruiz-Tijerina et al. who proved that increasing the gate voltage would produce a visible decay in the zero bias conductance down to $\frac{0.5e^2}{h}$ (See Figure 5.6). Hence, allowing to measure the Majorana signature without the superposition with the Kondo peak. This result is clear from Figure 5.5. At $\Delta\epsilon = 0$ the DOS at the Fermi energy is $\frac{1}{\pi\Gamma_1}$ for spin- \uparrow and $\frac{0.5}{\pi\Gamma_1}$ for spin- \downarrow . Instead, at big $\Delta\epsilon_1$ the only $\frac{0.5}{\pi\Gamma_1}$ spin- \downarrow peak appear. Since the zero bias conductance at zero temperature is essentially the sum of both spectral densities (times unit correction), Figure 5.5 recovers the results in Figure 5.6.

Another possibility to distinguish Kondo and Majorana physics is quenching the Kondo effect with a strong magnetic field. Similar to what was observed in Figure 5.6, the Kondo peak will be destroyed while the Majorana signature remains stable [1].

In the next chapter we will use these ideas to study the model of DQD attached to a Majorana

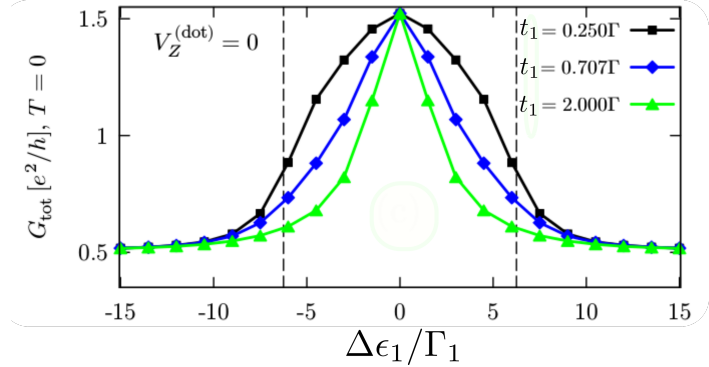


Figure 5.6: Dependence of the zero-bias conductance over tuning voltage

Source: Adapted from [1].

zero mode.

Chapter 6

Conclusions

All in all, we were able to develop two methods to study the model of double quantum dot coupled to a Majorana chain. We probed successfully these methods in simpler cases such as the double quantum dot (?? , ??) and the QD-Majorana system (chapter 5). The results obtained in these sections are in agreement with previous papers regarding the Kondo interference in double quantum dots [40], MZM leaking into quantum dots [26] and the co-existence of Kondo-Majorana physics [1].

Moreover, we introduced the Graph-Gauss-Jordan algorithm (??) as a simple, didactic, analytical and graphical method to solve the equations of motion. This method allowed us to obtain exact expressions for the non-interacting Green functions at several stages of the project. In particular, in the double quantum dot - Majorana model it proofed to be extremely useful to simplify the complexity of the solution given by a fractional polynomial of 9th-degree in up to 7 variables. With this expression we were able to predict interesting results to simulate in the non-interacting regime. We hope for its extended use in condensed matter physics.

In ?? we used the methods from chapter ?? to study the transitions of the Majorana zero modes inside a double quantum dots. Comparing the exact analytical solution in the non-interacting system and the NRG results for interacting quantum dots, we were able to characterized the displacements of the MZM inside the double quantum dot for the three setups in FIG.???. All these manipulations are summarized in Figure 6.1 . We observe a considerable agreement regarding the location of the Majorana signature between the interacting and non-interacting results with minor differences:

Figure 6.1(a): In the symmetric coupling the MZM leaks inside both dots. For interacting dots, the Majorana signature will emerge near the Kondo temperature. At this regime the system presents combined Kondo-Majorana physics . Additional satellite peaks produced by the indirect exchange through the lead and the MZM appear at low energies. If the gate voltage of one dot is turned on the MZM is induced to tunnel only into the other dot, which is the key to MZM manipulation.

??(b): In this system the spin- \uparrow zero mode at QD1 (The Kondo peak if the system is interacting) is destroyed by quantum interference with the second dot. This interference will also destroy the MZM in the first dot but a type I Majorana signature will still appear in the second dot. The Majorana mode can be induced to tunnel back into the first dot if a gate voltage is applied on the second dot. This signature is visible at very low energies (below $0.1\Gamma_1$) in the interacting case.

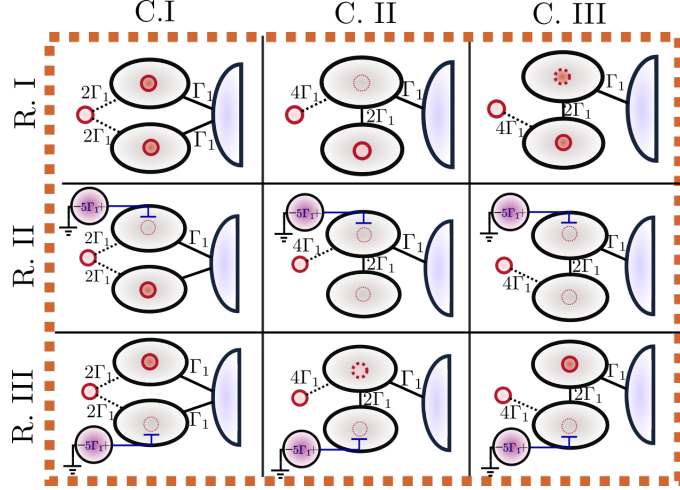


Figure 6.1: Table of Majorana signatures in the studied cases .

??(c): An indirect type II Majorana signature is observed in the first dot. This signature is robust, specially in the interacting case, where it is present in all configurations, despite gate voltage tuning.

Besides MZM manipulation we also pointed out other cases that could lead to future projects, such as the separation of the exchange interactions produced through the lead and through the MZM, the emergence of an indirect Majorana signature passing through the leads and the critical behavior in the T-dot junction when a gate voltage is applied on the second dot.

Bibliography

- [1] David A. Ruiz-Tijerina, E. Vernek, Luis G. G. V. Dias da Silva, and J. C. Egues. Interaction effects on a majorana zero mode leaking into a quantum dot. 91(11):115435. doi: 10.1103/PhysRevB.91.115435. URL <https://link.aps.org/doi/10.1103/PhysRevB.91.115435>. 1, 2, 2, 4, 5.1, 5.3, 5.6, 6
- [2] A. Yu Kitaev. Unpaired Majorana fermions in quantum wires. *Phys.-Usp.*, 44(10S):131, 2001. ISSN 1063-7869. doi: 10.1070/1063-7869/44/10S/S29. URL <http://stacks.iop.org/1063-7869/44/i=10S/a=S29>. 3
- [3] Frank Wilczek. Majorana returns, September 2009. URL <https://www.nature.com/articles/nphys1380>. 3
- [4] Jiannis K. Pachos. *Introduction to Topological Quantum Computation*. Cambridge University Press, Cambridge ; New York, 1 edition edition, May 2012. ISBN 978-1-107-00504-4. 3, 3.1.2
- [5] Vladimir G. Turaev. *Quantum Invariants of Knots and 3-Manifolds*. De Gruyter, Berlin, Boston, 3rd corr. ed. edition, 2016. ISBN 978-3-11-043522-1. URL <https://www.degruyter.com/view/product/461906>. 3, 3.1.2
- [6] Liang Fu and C. L. Kane. Superconducting Proximity Effect and Majorana Fermions at the Surface of a Topological Insulator. *Phys. Rev. Lett.*, 100(9):096407, March 2008. doi: 10.1103/PhysRevLett.100.096407. URL <https://link.aps.org/doi/10.1103/PhysRevLett.100.096407>. 3
- [7] Masatoshi Sato, Yoshiro Takahashi, and Satoshi Fujimoto. Non-Abelian Topological Order in \$s\$-\$s\$-Wave Superfluids of Ultracold Fermionic Atoms. *Phys. Rev. Lett.*, 103(2):020401, July 2009. doi: 10.1103/PhysRevLett.103.020401. URL <https://link.aps.org/doi/10.1103/PhysRevLett.103.020401>.
- [8] Jason Alicea. New directions in the pursuit of Majorana fermions in solid state systems. *Rep. Prog. Phys.*, 75(7):076501, 2012. ISSN 0034-4885. doi: 10.1088/0034-4885/75/7/076501. URL <http://stacks.iop.org/0034-4885/75/i=7/a=076501>. 3.1.1, 3.6, 3.1.3

BIBLIOGRAPHY

- [9] C.w.j. Beenakker. Search for Majorana Fermions in Superconductors. *Annual Review of Condensed Matter Physics*, 4(1):113–136, March 2013. ISSN 1947-5454. doi: 10.1146/annurev-conmatphys-030212-184337. URL <https://www.annualreviews.org/doi/10.1146/annurev-conmatphys-030212-184337>. 3
- [10] V. Mourik, K. Zuo, S. M. Frolov, S. R. Plissard, E. P. a. M. Bakkers, and L. P. Kouwenhoven. Signatures of Majorana Fermions in Hybrid Superconductor-Semiconductor Nanowire Devices. *Science*, 336(6084):1003–1007, May 2012. ISSN 0036-8075, 1095-9203. doi: 10.1126/science.1222360. URL <http://science-sciencemag.org.ez67.periodicos.capes.gov.br/content/336/6084/1003>. 3, 3.1.3
- [11] Anindya Das, Yuval Ronen, Yonatan Most, Yuval Oreg, Moty Heiblum, and Hadas Shtrikman. Zero-bias peaks and splitting in an Al-InAs nanowire topological superconductor as a signature of Majorana fermions. *Nature Physics*, 8(12):887, December 2012. ISSN 1745-2481. doi: 10.1038/nphys2479. URL <https://www.nature.com/articles/nphys2479>. 3.1.3
- [12] M. T. Deng, C. L. Yu, G. Y. Huang, M. Larsson, P. Caroff, and H. Q. Xu. Anomalous Zero-Bias Conductance Peak in a Nb-InSb Nanowire-Nb Hybrid Device. *Nano Letters*, 12(12):6414–6419, December 2012. ISSN 1530-6984. doi: 10.1021/nl303758w. URL <http://dx.doi.org/10.1021/nl303758w>.
- [13] M. T. Deng, S. Vaitiekėnas, E. B. Hansen, J. Danon, M. Leijnse, K. Flensberg, J. Nygård, P. Krogstrup, and C. M. Marcus. Majorana bound state in a coupled quantum-dot hybrid-nanowire system. 354(6319):1557–1562. ISSN 0036-8075, 1095-9203. doi: 10.1126/science.aaf3961. URL <http://science.sciencemag.org/content/354/6319/1557>. 3.2
- [14] Hao Zhang, Chun-Xiao Liu, Sasa Gazibegovic, Di Xu, John A. Logan, Guanzhong Wang, Nick van Loo, Jouri D. S. Bommer, Michiel W. A. de Moor, Diana Car, Roy L. M. Op het Veld, Petrus J. van Veldhoven, Sebastian Koelling, Marcel A. Verheijen, Mihir Pendharkar, Daniel J. Pennachio, Borzoyeh Shojaei, Joon Sue Lee, Chris J. Palmstrom, Erik P. A. M. Bakkers, S. Das Sarma, and Leo P. Kouwenhoven. Quantized Majorana conductance. *Nature*, 556:74, March 2018. URL <http://dx.doi.org/10.1038/nature26142>. 3, 3.1.3, 3.7
- [15] Yuval Oreg, Gil Refael, and Felix von Oppen. Helical Liquids and Majorana Bound States in Quantum Wires. *Physical Review Letters*, 105(17):177002, October 2010. doi: 10.1103/PhysRevLett.105.177002. URL <https://link.aps.org/doi/10.1103/PhysRevLett.105.177002>. 3
- [16] Roman M. Lutchyn, Jay D. Sau, and S. Das Sarma. Majorana Fermions and a Topological Phase Transition in Semiconductor-Superconductor Heterostructures. *Physical Re-*

BIBLIOGRAPHY

- view Letters*, 105(7):077001, August 2010. doi: 10.1103/PhysRevLett.105.077001. URL <https://link.aps.org/doi/10.1103/PhysRevLett.105.077001>. 3, 3.1.3
- [17] Shinsei Ryu, Andreas P. Schnyder, Akira Furusaki, and Andreas W. W. Ludwig. Topological insulators and superconductors: tenfold way and dimensional hierarchy. *New Journal of Physics*, 12(6):065010, June 2010. ISSN 1367-2630. doi: 10.1088/1367-2630/12/6/065010. URL <https://doi.org/10.1088%2F1367-2630%2F12%2F6%2F065010>. 3.1.1
- [18] Chetan Nayak, Steven H. Simon, Ady Stern, Michael Freedman, and Sankar Das Sarma. Non-Abelian anyons and topological quantum computation. *Reviews of Modern Physics*, 80(3):1083–1159, September 2008. doi: 10.1103/RevModPhys.80.1083. URL <https://link.aps.org/doi/10.1103/RevModPhys.80.1083>. 3.1.2
- [19] A. Manchon, H. C. Koo, J. Nitta, S. M. Frolov, and R. A. Duine. New perspectives for Rashba spin-orbit coupling. *Nature Materials*, 14(9):871–882, September 2015. ISSN 1476-4660. doi: 10.1038/nmat4360. URL <https://www.nature.com/articles/nmat4360>. 3.1.3
- [20] Stevan Nadj-Perge, Ilya K. Drozdov, Jian Li, Hua Chen, Sangjun Jeon, Jungpil Seo, Allan H. MacDonald, B. Andrei Bernevig, and Ali Yazdani. Observation of Majorana fermions in ferromagnetic atomic chains on a superconductor. *Science*, 346(6209):602–607, October 2014. ISSN 0036-8075, 1095-9203. doi: 10.1126/science.1259327. URL <http://science.sciencemag.org/content/346/6209/602>. 3.1.3
- [21] S. Das Sarma, Jay D. Sau, and Tudor D. Stanescu. A Majorana smoking gun for the superconductor-semiconductor hybrid topological system. *Physical Review B*, 86(22), December 2012. ISSN 1098-0121, 1550-235X. doi: 10.1103/PhysRevB.86.220506. URL <http://arxiv.org/abs/1211.0539>. arXiv: 1211.0539. 3.1.3
- [22] G. Górski, J. Barański, I. Weymann, and T. DomaÅski. Interplay between correlations and Majorana mode in proximitized quantum dot. *Scientific Reports*, 8(1):15717, October 2018. ISSN 2045-2322. doi: 10.1038/s41598-018-33529-1. URL <https://www.nature.com/articles/s41598-018-33529-1>. 3.1.3, 2, 2
- [23] David Aasen, Michael Hell, Ryan V. Mishmash, Andrew Higginbotham, Jeroen Danon, Martin Leijnse, Thomas S. Jespersen, Joshua A. Folk, Charles M. Marcus, Karsten Flensberg, and Jason Alicea. Milestones Toward Majorana-Based Quantum Computing. *Physical Review X*, 6(3):031016, August 2016. doi: 10.1103/PhysRevX.6.031016. URL <https://link.aps.org/doi/10.1103/PhysRevX.6.031016>. 3.1.3
- [24] Sankar Das Sarma, Michael Freedman, and Chetan Nayak. Majorana zero modes and topological quantum computation. *npj Quantum Information*, 1:15001, October 2015. ISSN 2056-6387. doi: 10.1038/npjqi.2015.1. URL <https://www.nature.com/articles/npjqi20151>.

BIBLIOGRAPHY

- [25] B. van Heck, A. R. Akhmerov, F. Hassler, M. Burrello, and C. W. J. Beenakker. Coulomb-assisted braiding of Majorana fermions in a Josephson junction array. *New Journal of Physics*, 14(3):035019, March 2012. ISSN 1367-2630. doi: 10.1088/1367-2630/14/3/035019. URL <https://doi.org/10.1088/1367-2630/14/3/035019>. 3.1.3
- [26] Dong E. Liu and Harold U. Baranger. Detecting a majorana-fermion zero mode using a quantum dot. 84(20). ISSN 1098-0121, 1550-235X. doi: 10.1103/PhysRevB.84.201308. URL <http://arxiv.org/abs/1107.4338>. 3.2, 3.3, 5, 5.1, 5.2, 6
- [27] E. Vernek, P. H. Penteado, A. C. Seridonio, and J. C. Egues. Subtle leakage of a majorana mode into a quantum dot. 89(16):165314. doi: 10.1103/PhysRevB.89.165314. URL <https://link.aps.org/doi/10.1103/PhysRevB.89.165314>. 3.2, 2, 5, 5.1
- [28] Eduardo J. H. Lee, Xiaocheng Jiang, Ramón Aguado, Georgios Katsaros, Charles M. Lieber, and Silvano De Franceschi. Zero-Bias Anomaly in a Nanowire Quantum Dot Coupled to Superconductors. *Physical Review Letters*, 109(18):186802, October 2012. doi: 10.1103/PhysRevLett.109.186802. URL <https://link.aps.org/doi/10.1103/PhysRevLett.109.186802>. 2
- [29] Minchul Lee, Jong Soo Lim, and Rosa Lopez. Kondo effect in a quantum dot side-coupled to a topological superconductor. 87(24):241402. doi: 10.1103/PhysRevB.87.241402. URL <https://link.aps.org/doi/10.1103/PhysRevB.87.241402>. 2, 2
- [30] Cornelius Malciu, Leonardo Mazza, and Christophe Mora. Braiding Majorana zero modes using quantum dots. *Physical Review B*, 98(16):165426, October 2018. doi: 10.1103/PhysRevB.98.165426. URL <https://link.aps.org/doi/10.1103/PhysRevB.98.165426>. 3, 3.8
- [31] Torsten Karzig, Christina Knapp, Roman M. Lutchyn, Parsa Bonderson, Matthew B. Hastings, Chetan Nayak, Jason Alicea, Karsten Flensberg, Stephan Plugge, Yuval Oreg, Charles M. Marcus, and Michael H. Freedman. Scalable designs for quasiparticle-poisoning-protected topological quantum computation with Majorana zero modes. *Physical Review B*, 95(23):235305, June 2017. doi: 10.1103/PhysRevB.95.235305. URL <https://link.aps.org/doi/10.1103/PhysRevB.95.235305>. 3.8, 3
- [32] Zhaoen Su, Alexandre B. Tacla, Moira Hocevar, Diana Car, Sébastien R. Plissard, Erik P. A. M. Bakkers, Andrew J. Daley, David Pekker, and Sergey M. Frolov. Andreev molecules in semiconductor nanowire double quantum dots. *Nature Communications*, 8(1):585, September 2017. ISSN 2041-1723. doi: 10.1038/s41467-017-00665-7. URL <https://www.nature.com/articles/s41467-017-00665-7>. 3.2, 3.2.1
- [33] Joelson F Silva and E Vernek. Andreev and majorana bound states in single and double quantum dot structures. *Journal of Physics: Condensed Matter*, 28(43):435702,

BIBLIOGRAPHY

- sep 2016. doi: 10.1088/0953-8984/28/43/435702. URL <https://doi.org/10.1088%2F0953-8984%2F28%2F43%2F435702>. 3.2.1
- [34] T. I. Ivanov. Coherent tunneling through a double quantum dot coupled to Majorana bound states. *Physical Review B*, 96(3):035417, July 2017. doi: 10.1103/PhysRevB.96.035417. URL <https://link.aps.org/doi/10.1103/PhysRevB.96.035417>. 3.2.1
- [35] M. A. Ruderman and C. Kittel. Indirect Exchange Coupling of Nuclear Magnetic Moments by Conduction Electrons. *Physical Review*, 96(1):99–102, October 1954. doi: 10.1103/PhysRev.96.99. URL <https://link.aps.org/doi/10.1103/PhysRev.96.99>. 3.2.1, A.2
- [36] Tadao Kasuya. A Theory of Metallic Ferro- and Antiferromagnetism on Zener’s Model. *Progress of Theoretical Physics*, 16(1):45–57, July 1956. ISSN 0033-068X. doi: 10.1143/PTP.16.45. URL <https://academic.oup.com/ptp/article/16/1/45/1861363>.
- [37] Kei Yosida. Magnetic Properties of Cu-Mn Alloys. *Physical Review*, 106(5):893–898, June 1957. doi: 10.1103/PhysRev.106.893. URL <https://link.aps.org/doi/10.1103/PhysRev.106.893>. 3.2.1, A.2
- [38] D. N. Zubarev. DOUBLE-TIME GREEN FUNCTIONS IN STATISTICAL PHYSICS. *Soviet Physics Uspekhi*, 3(3):320, 1960. ISSN 0038-5670. doi: 10.1070/PU1960v003n03ABEH003275. URL <http://iopscience.iop.org/article/10.1070/PU1960v003n03ABEH003275/meta>. 3.3
- [39] Kenneth G. Wilson. The renormalization group: Critical phenomena and the Kondo problem. *Reviews of Modern Physics*, 47(4):773–840, October 1975. doi: 10.1103/RevModPhys.47.773. URL <https://link.aps.org/doi/10.1103/RevModPhys.47.773>. 3.3
- [40] Luis G. G. V. Dias da Silva, Nancy Sandler, Kevin Ingersent, and Sergio E. Ulloa. Transmission in double quantum dots in the Kondo regime: Quantum-critical transitions and interference effects. *Physica E: Low-dimensional Systems and Nanostructures*, 40(5):1002–1005, March 2008. ISSN 1386-9477. doi: 10.1016/j.physe.2007.08.098. URL <http://www.sciencedirect.com/science/article/pii/S1386947707003074>. 3.3, 6
- [41] Alexander W. Holleitner, Robert H. Blick, Andreas K. Huttel, Karl Eberl, and Jorg P. Kotthaus. Probing and Controlling the Bonds of an Artificial Molecule. *Science*, 297(5578):70–72, July 2002. ISSN 0036-8075, 1095-9203. doi: 10.1126/science.1071215. URL <http://science.scienmag.org/content/297/5578/70>. 4.1
- [42] Dieter Bimberg, Marius Grundmann, and Nikolai N. Ledentsov. *Quantum Dot Heterostructures*. Wiley, Chichester, Eng.; New York, 1 edition, March 1999. ISBN 978-0-471-97388-1. 4.1, 4.1

BIBLIOGRAPHY

- [43] Michael Sindel. *Numerical Renormalization Group studies of Quantum Impurity Models in the Strong Coupling Limit.* Text.PhDThesis, Ludwig-Maximilians-Universitat Munchen, January 2005. URL <https://edoc.ub.uni-muenchen.de/3115/>. 4.1, 4.3, 4.2, A.1
- [44] P. W. Anderson. Localized Magnetic States in Metals. *Physical Review*, 124(1):41–53, October 1961. doi: 10.1103/PhysRev.124.41. URL <https://link.aps.org/doi/10.1103/PhysRev.124.41>. 4.2
- [45] W.J. de Haas, J. de Boer, and G.J. van dĂ n Berg. The electrical resistance of gold, copper and lead at low temperatures. *Physica*, 1(7):1115 – 1124, 1934. ISSN 0031-8914. doi: [https://doi.org/10.1016/S0031-8914\(34\)80310-2](https://doi.org/10.1016/S0031-8914(34)80310-2). URL <http://www.sciencedirect.com/science/article/pii/S0031891434803102>. 4.4, 4.3
- [46] Markus Ternes, Andreas J Heinrich, and Wolf-Dieter Schneider. Spectroscopic manifestations of the kondo effect on single adatoms. *Journal of Physics: Condensed Matter*, 21(5):053001, dec 2008. doi: 10.1088/0953-8984/21/5/053001. URL <https://doi.org/10.1088%2F0953-8984%2F21%2F5%2F053001>. 4.4
- [47] Alexander Cyril Hewson. *The Kondo Problem to Heavy Fermions*. Cambridge University Press, April 1997. ISBN 978-0-521-59947-4. Google-Books-ID: fPzgHneNFDAC. 4.3
- [48] W. G. van der Wiel, S. De Franceschi, T. Fujisawa, J. M. Elzerman, S. Tarucha, and L. P. Kouwenhoven. The Kondo Effect in the Unitary Limit. *Science*, 289(5487):2105–2108, September 2000. ISSN 0036-8075, 1095-9203. doi: 10.1126/science.289.5487.2105. URL <http://science-scienmag-org.ez67.periodicos.capes.gov.br/content/289/5487/2105>. 4.5
- [49] D. Goldhaber-Gordon, Hadas Shtrikman, D. Mahalu, David Abusch-Magder, U. Meirav, and M. A. Kastner. Kondo effect in a single-electron transistor. *Nature*, 391(6663):156–159, January 1998. ISSN 1476-4687. doi: 10.1038/34373. URL <https://www.nature.com/articles/34373>. 4.3.1
- [50] Maissam Barkeshli and Jay D. Sau. Physical Architecture for a Universal Topological Quantum Computer based on a Network of Majorana Nanowires. *arXiv:1509.07135 [cond-mat, physics:quant-ph]*, September 2015. URL <http://arxiv.org/abs/1509.07135>. arXiv: 1509.07135. 3
- [51] H. R. Krishna-murthy, J. W. Wilkins, and K. G. Wilson. Renormalization-group approach to the Anderson model of dilute magnetic alloys. 1. Static properties for the symmetric case. *Phys.Rev.*, B21:1003–1043, 1980. doi: 10.1103/PhysRevB.21.1003. A.1, A.1
- [52] Ralf Bulla, Theo A. Costi, and Thomas Pruschke. Numerical renormalization group method for quantum impurity systems. *Reviews of Modern Physics*, 80(2):395–450,

April 2008. doi: 10.1103/RevModPhys.80.395. URL <https://link.aps.org/doi/10.1103/RevModPhys.80.395>. A.1

Appendix A

Appendix

A.1 From the logarithmic discretization to the Wilson's chain.

Logarithmic Discretization:

We start with an Anderson model Hamiltonian such as the one in (4.5) without magnetic field

$$H = \frac{U}{2} + \sum_{\sigma} \left[\left(\varepsilon_d + \frac{U}{2} \right) d_{\sigma}^{\dagger} d_{\sigma} + \frac{U}{2} (d_{\sigma}^{\dagger} d_{\sigma} - 1)^2 + \sum_{\mathbf{k}} \varepsilon_{\mathbf{k}} c_{\mathbf{k}\sigma}^{\dagger} c_{\mathbf{k}\sigma} + V_{\mathbf{k}} d_{\sigma}^{\dagger} c_{\mathbf{k}\sigma} + V_{\mathbf{k}}^* c_{\mathbf{k}\sigma}^{\dagger} d_{\sigma} \right]. \quad (\text{A.1})$$

At low-energies we can assume that QD couples only to s-wave states in the leads[51]. This implies that that the Fermi surface is contained in a single, isotropic conduction band extending inside some fixed cutoffs $-D$ and D . Thus, $\varepsilon_{\mathbf{k}}$ only depends on $|\mathbf{k}|$. This makes possible to transform the sum over \mathbf{k} in equation A.1 into an integral over ε between the energy cutoffs

$$\begin{aligned} H = \sum_{\sigma} & \left[\left(\varepsilon_d + \frac{U}{2} \right) d_{\sigma}^{\dagger} d_{\sigma} + \frac{U}{2} (d_{\sigma}^{\dagger} d_{\sigma} - 1)^2 + \int_{-D}^D d\varepsilon \varepsilon c_{\varepsilon\sigma}^{\dagger} c_{\varepsilon\sigma} \right. \\ & \left. + \int_{-D}^D \sqrt{\rho_{\sigma}(\varepsilon)} d\varepsilon V_{\varepsilon} d_{\sigma}^{\dagger} c_{\mathbf{k}\sigma} + V_{\varepsilon}^* c_{\varepsilon\sigma}^{\dagger} d_{\sigma} \right]. \end{aligned} \quad (\text{A.2})$$

Here $c_{\varepsilon\sigma}^{\dagger}$ creates an electron with energy ε and $\rho_{\sigma}(\varepsilon)$ is the density of states of the system per spin, which appears in the integral due to the change of variable from \mathbf{k} to $\varepsilon \propto |\mathbf{k}|^2$. Finally, we ignore the energy dependence of ρ and V_d and we replace them by their values in the Fermi energy (This approximation has no great relevance which is justified in [51]) and we renormalize the energy band doing the replacements $k = \frac{\varepsilon}{D}$ and $c_{k\sigma} := \sqrt{D} c_{\varepsilon\sigma}$ so that (A.2) becomes

$$H = D \sum_{\sigma} \left[\frac{1}{D} \left(\varepsilon_d + \frac{U}{2} \right) d_{\sigma}^{\dagger} d_{\sigma} + \frac{U}{2D} (d_{\sigma}^{\dagger} d_{\sigma} - 1)^2 + \int_{-1}^1 dk k c_{k\sigma}^{\dagger} c_{k\sigma} + \sqrt{\frac{\Gamma}{\pi D}} \int_{-1}^1 dk d_{\sigma}^{\dagger} c_{k\sigma} + c_{k\sigma}^{\dagger} d_{\sigma} \right] \quad (\text{A.3})$$

$$= H_d + D \sum_{\sigma} \left[\int_{-1}^1 dk k c_{k\sigma}^{\dagger} c_{k\sigma} + \sqrt{\frac{\Gamma}{\pi D}} \int_{-1}^1 dk d_{\sigma}^{\dagger} c_{k\sigma} + c_{k\sigma}^{\dagger} d_{\sigma} \right], \quad (\text{A.4})$$

where $\Gamma = \pi \rho V^2$ is associated to the lever-width [43, (3.5)]. At this point we have our model dependent of three unit-less constants $\frac{\varepsilon_d}{D}$, $\frac{U}{2D}$ and $\frac{\Gamma}{\pi D}$. The logarithmic discretization starts by defining an scaling parameter $\Lambda \geq 1$ in diving the energy domain $[-1, 1]$ into an array of intervals of the form $\{[\pm \Lambda^{-(n+1)}, \pm \Lambda^n]\}_{n \in \mathbb{N}}$, as we can observe in ???. Note that the width of these intervals is decreasing exponentially by

$$d_n = \Lambda^{-n} (1 - \Lambda^{-1}).$$

Then inside of these energy intervals we can define a set of orthonormal Fourier series of the form

$$\phi_{np}^{\pm}(\varepsilon) = \begin{cases} \frac{1}{\sqrt{d_n}} e^{\pm i \omega_n p \varepsilon} & \varepsilon \in [\pm \Lambda^{-(n+1)}, \pm \Lambda^n] \\ 0 & \text{a.o.c.} \end{cases} \quad (\text{A.5})$$

with $\omega_n := \frac{2\pi}{d_n}$ so that $\phi_{np}^{\pm}(\pm \Lambda^{-(n+1)}) = \phi_{np}^{\pm}(\pm \Lambda^{-n})$. Then we can decompose the creation operators c_k^{\dagger} into their interval-Fourier contributions as

$$c_k^{\dagger} = \sum_{np} \phi_{np}^{+}(k) c_{np\sigma}^{+\dagger} + \phi_{np}^{-}(k) c_{np\sigma}^{-\dagger} \quad (\text{A.6})$$

with the new creation operators defined as

$$c_{np\sigma}^{\pm\dagger} := (c_{np\sigma}^{\pm})^{\dagger} = \int_{-1}^1 d\varepsilon [\phi_{np}^{+}(\varepsilon)]^* c_{\varepsilon\sigma}^{\dagger}.$$

This decomposition (A.6) is a simple consequence of the orthonormality of the functions defined in (A.5). In addition we can readily proof that $c_{np\sigma}^{\pm\dagger}$ -operators satisfy the anti-commutation relations, so that they are rightful fermionic creation operators.

We can now use (A.6) to replace the k -dependent terms in hamiltonian (A.3). Then we obtain

$$\begin{aligned}
\int_{-1}^1 dk c_{k\sigma}^\dagger d_\sigma &= \int_{-1}^1 dk \left(\sum_{np} \phi_{np}^+(k) c_{np\sigma}^{+\dagger} + \phi_{np}^-(k) c_{np\sigma}^{-\dagger} \right) d_\sigma \\
&= \left(\sum_{np} \left(\int_{-1}^1 dk \phi_{np}^+(k) \right) c_{np\sigma}^{+\dagger} + \left(\int_{-1}^1 dk \phi_{np}^-(k) \right) c_{np\sigma}^{-\dagger} \right) d_\sigma \\
&= \left(\sum_{np} \left(\int_{\Lambda^{-(n+1)}}^{\Lambda^{-n}} dk \frac{e^{i\omega_n p k}}{\sqrt{d_n}} \right) c_{np\sigma}^{+\dagger} + \left(\int_{-\Lambda^{-n}}^{-\Lambda^{-(n+1)}} dk \frac{e^{-i\omega_n p k}}{\sqrt{d_n}} \right) c_{np\sigma}^{-\dagger} \right) d_\sigma \\
&= \left(\sum_{np} \sqrt{d_n} \delta_p c_{np\sigma}^{+\dagger} + \sqrt{d_n} \delta_p c_{np\sigma}^{-\dagger} \right) d_\sigma \\
&= \sqrt{1 - \Lambda^{-1}} \sum_n \Lambda^{-\frac{n}{2}} (c_{np\sigma}^{+\dagger} + c_{np\sigma}^{-\dagger}) d_\sigma. \tag{A.7}
\end{aligned}$$

And

$$\begin{aligned}
\int_{-1}^1 dk k c_{k\sigma}^\dagger c_{k\sigma} &= \sum_{n,n',p,p'} \sum_{s,s'=\pm} \left(\int_{-1}^1 k dk \phi_{np}^s(k) (\phi_{np}^{s'}(k))^* \right) c_{np\sigma}^{s\dagger} c_{n'p'\sigma}^{s'} \\
&= \sum_{n,n',p,p'} \sum_{s,s'=\pm} \left(\frac{\delta_{nn'} \delta_{ss'}}{d_n} \int_{\Lambda^{-(n+1)}}^{\Lambda^{-n}} k dk e^{is\omega_n k(p-p')} \right) c_{np\sigma}^{s\dagger} c_{n'p'\sigma}^s \\
&= \sum_{npp'} \sum_{s=\pm} \left(\frac{s}{2} \Lambda^{-2n} (1 - \Lambda^{-2}) \delta_{pp'} + \frac{1 - \delta_{pp'}}{is\omega_n(p-p')} [ke^{is\omega_n k(p-p')}]_{\Lambda^{-(n+1)}}^{\Lambda^{-n}} \right) \frac{c_{np\sigma}^{s\dagger} c_{n'p'\sigma}^{s'}}{d_n} \\
&= \frac{1}{2} (1 + \Lambda^{-1}) \sum_{np} \Lambda^{-n} (c_{np\sigma}^{+\dagger} c_{np\sigma}^+ - c_{np\sigma}^{-\dagger} c_{np\sigma}^-) \\
&\quad + \sum_n \sum_{p \neq p'} \frac{1 - \Lambda^{-1}}{2i\pi(p' - p)} (c_{np\sigma}^{+\dagger} c_{np'\sigma}^+ - c_{np'\sigma}^{-\dagger} c_{np\sigma}^-) e^{\frac{2i\pi(p-p')}{1-\Lambda^{-1}}}. \tag{A.8}
\end{aligned}$$

Thus, if we replace (A.7) and (A.8) into (A.3) we will obtain a logarithmic discretization of the hamiltonian. The next part will we to map this discretization to an iterative process that is worth for a numerical computations.

Mapping the Anderson model to a Chain-Hamiltonian

We are looking for a model just like the one we have in the right part of ???. This is because a Chain-Hamiltonian will give an iterative approximation of the Anderson model with an increasing (but still controllable) number of degrees of freedom. This will provide the rightful structure for a numerical diagonalization of the hamiltonian.

A.1. From the logarithmic discretization to the Wilson's chain.

To do this, observe from equations (A.7),(A.8) that the QD (d_σ) couples directly only to the operators with $p = 0$ ($c_{n0\sigma}^{\pm\dagger}$). The $p \neq 0$ terms will appear in the hamiltonian only because they are coupled to $c_{np\sigma}^{+\dagger}$ in Equation (A.8). Thus, as a first approximation we can neglect all terms in (A.8) with $p \neq 0$. This leaves only the first part of (A.8), so that we can define $c_{n\sigma}^{\pm\dagger} := c_{np\sigma}^{\pm\dagger}$. Let

$$f_{0\sigma}^\dagger = \sqrt{\frac{1-\Lambda^{-1}}{2}} \sum_n \Lambda^{-\frac{n}{2}} (c_{n\sigma}^{+\dagger} + c_{n\sigma}^{-\dagger}), \text{ so that } \sqrt{2} f_{0\sigma}^\dagger d_\sigma = \int_{-1}^1 dk c_{k\sigma}^\dagger d_\sigma. \quad (\text{A.9})$$

Note $\{f_{0\sigma}^\dagger, f_{0\sigma}\} = \frac{1-\Lambda^{-1}}{2} \sum_n 2\Lambda^{-n} = 1$. Replacing this in (A.3)we get

$$H = H_d + D \sum_\sigma \left[\sqrt{\frac{2\Gamma}{\pi D}} (d_\sigma^\dagger f_{0\sigma} + f_{0\sigma}^\dagger d_\sigma) + \frac{1}{2} (1 + \Lambda^{-1}) \sum_n \Lambda^{-n} (c_{n\sigma}^{+\dagger} c_{n\sigma}^+ - c_{n\sigma}^{-\dagger} c_{n\sigma}^-) \right].$$

f_0^\dagger will represent the first site of the chain-hamiltonian in ?? since no other term is coupled to the dot hamiltonian. We also have the coupling term $\xi_0 = \sqrt{\frac{2\Gamma}{\pi D}}$. It is possible to obtain the following f_m^\dagger -operators by supposing a solution of the form

$$f_{m\sigma}^\dagger = \sum_n a_{mn}^+ c_{n\sigma}^{+\dagger} + a_{mn}^- c_{n\sigma}^{-\dagger} = \sum_n \sum_{s=\pm} a_{mn}^s c_{n\sigma}^{s\dagger}, \quad (\text{A.10})$$

such that they satisfy the anti-commutation relations

$$\{f_{m\sigma}^\dagger, f_{m\sigma}\} = \delta_{mm'} \delta_{\sigma\sigma'}, \quad \{f_{m\sigma}^\dagger, f_{m'\sigma'}^\dagger\} = \{f_{m\sigma}^\dagger, f_{m\sigma}^\dagger\} = 0$$

and

$$\frac{1}{2} (1 + \Lambda^{-1}) \sum_n \Lambda^{-n} (c_{n\sigma}^{+\dagger} c_{n\sigma}^+ - c_{n\sigma}^{-\dagger} c_{n\sigma}^-) = \sum_{m=0}^{\infty} \Lambda^{\frac{-m}{2}} \xi_m (f_{m\sigma}^\dagger f_{m+1,\sigma} + f_{m+1,\sigma}^\dagger f_{m\sigma}). \quad (\text{A.11})$$

It is possible to find a solution for this system using the formula of the right part of equation A.11. Since the relation is only given between consecutive terms $m, m+1$ and we already have the coefficients for $m = 0$ ($a_{0n}^s = \sqrt{\frac{1-\Lambda^{-1}}{2}} \Lambda^{-\frac{n}{2}}$). Then it is possible to determine the upper coefficients in a recursive way starting from $m = 0$. Supposing we can obtain the m^{th} -coefficients (a_{mn}^s) and then finding iteratively the coefficients of $m+1$ ($a_{m+1,n}^s$) using the relation given by equation (A.11). This provides a numerical way for obtaining the $f_{m\sigma}^\dagger$ operators. In fact in our case, where we actually did important assumptions, the problem can be solved analytically obtaining that the final Hamiltonian is given by

$$H = H_d + D \sum_\sigma \left[\sqrt{\frac{2\Gamma}{\pi D}} (d_\sigma^\dagger f_{0\sigma} + f_{0\sigma}^\dagger d_\sigma) + \frac{1}{2} (1 + \Lambda^{-1}) \sum_{n=0}^{\infty} \Lambda^{\frac{-n}{2}} \xi_n (f_{n\sigma}^\dagger f_{n+1,\sigma} + f_{n+1,\sigma}^\dagger f_{n\sigma}) \right]. \quad (\text{A.12})$$

with

$$\xi_n = \frac{1 - \Lambda^{-n-1}}{(1 - \Lambda^{-2n-1})^{\frac{1}{2}} (1 - \Lambda^{-2n-3})^{\frac{1}{2}}}.$$

The formal recursive-solution of this problem can be found in [52]. Note that equation (A.12) describes the chain hamiltonian model that we where looking for in ???. Note that in the limit when $n \rightarrow \infty$

$$\Lambda^{\frac{-n}{2}} \xi_n \rightarrow \frac{\Lambda^{\frac{-n}{2}} (1 - \Lambda^{-n})}{1 - \Lambda^{-2n}} \sim \frac{\Lambda^{\frac{-n}{2}}}{1 + \Lambda^{-n}},$$

which implies an exponential decaying of the hopping term in the chain.

A.2 Three peak appearance in the Double Quantum Dot model.

The DQD model is characterized by the formation of a new state that entangles the two Quantum dots through the leads. This produces an anti-ferromagnetic interaction between the QDs, commonly known as Ruderman-Kittel-Kasuya-Yosida (RKKY) interaction [35, 37]. As consequence, two satellite peaks will emerge in the Density of States.

To explain this phenomenon we will take a symmetric version of Hamiltonian (??) with $2e_i = U_i = U$, $t_i = t$ and $t_{dots} = 0$ for $i \in \{1, 2\}$.

$$H = \sum_{i,k,\sigma} \frac{U_i}{2} (d_{i\sigma}^\dagger d_{i\sigma} - 1)^2 + t(d_{+,+} + d_{+,-}^\dagger) \gamma_1 + \Gamma_i (d_{i\sigma}^\dagger c_{k\sigma} + c_{k\sigma}^\dagger d_{i\sigma}). \quad (\text{A.13})$$

The symmetry of the previous Hamiltonian is suitable to apply a base change of the form

$$d_{+,\sigma} = \frac{1}{\sqrt{2}}(d_{1\sigma} + d_{2\sigma}), \quad d_{-,\sigma} = \frac{1}{\sqrt{2}}(d_{1\sigma} - d_{2\sigma}).$$

These new operators satisfy the fermionic anti-commutation relations

$$\{d_{\pm,\sigma}, d_{\pm,\sigma}^\dagger\} = 1, \{d_{\pm,\sigma}, d_{\mp,\sigma}^\dagger\} = 0,$$

so that the may be considered as fermion operators. All lineal terms in (A.13) are trivially adapted to the new base. The repulsion potential

$$\sum_i (\sum_\sigma d_{i\sigma}^\dagger d_{i\sigma} - 1)^2 = (\sum_\sigma d_{1\sigma}^\dagger d_{1\sigma} - 1)^2 + (\sum_\sigma d_{2\sigma}^\dagger d_{2\sigma} - 1)^2.$$

gives rise to a non-trivial interaction between the new states. To find this interaction we define the particle number operator

$$\hat{n}_{i,\sigma} := d_{i,\sigma}^\dagger d_{i,\sigma}.$$

A.3. Initial DQD-Majorana Hamiltonian.

So that

$$\hat{n}_{1,\sigma} = \frac{1}{2} (\hat{n}_{+,\sigma} + \hat{n}_{-,\sigma} + d_{+,\sigma}^\dagger d_{-,\sigma} + d_{-,\sigma}^\dagger d_{+,\sigma}) = \frac{1}{2} (\hat{N}_\sigma + \hat{E}_\sigma),$$

with $\hat{N} = \hat{n}_{+,\sigma} + \hat{n}_{-,\sigma}$ and $\hat{E}_\sigma = d_{+,\sigma}^\dagger d_{-,\sigma} + d_{-,\sigma}^\dagger d_{+,\sigma}$. Similarly

$$\hat{n}_{2,\sigma} = \frac{1}{2} (\hat{N}_\sigma - \hat{E}_\sigma).$$

Hence

$$\sum_i (\sum_\sigma d_{i\sigma}^\dagger d_{i\sigma} - 1)^2 = \left(\frac{\hat{N} + \hat{E}}{2} - 1 \right)^2 + \left(\frac{\hat{N} - \hat{E}}{2} - 1 \right)^2 = \frac{(\hat{N} - 2)^2 - \hat{E}^2}{2},$$

with $\hat{N} = \sum_\sigma \hat{N}_\sigma$, $\hat{E} = \sum_\sigma \hat{E}_\sigma$. Note that opeator \hat{N} represents the total occupation number inside both dots. If this occupation is different than 2 there is an imbalance between particles and dots that is punished by this term. The term E^2 is much more interesting since this one is the responsible for the emergence of satellite peaks in the DOS. To understand what it makes it is simple to observe its results when applied to a based ordered by $|+, -\rangle$.

$$\begin{aligned} \hat{E}^2 |\uparrow, 0\rangle &= \hat{E} |0, \uparrow\rangle = |\uparrow, 0\rangle \\ \hat{E}^2 |\uparrow, \downarrow\rangle &= \hat{E} (|0, \uparrow\rangle + |\uparrow, 0\rangle) = 2|\uparrow, \downarrow\rangle - 2|\downarrow, \uparrow\rangle \end{aligned}$$

The new Hamiltonian

$$H = \sum_\sigma \frac{U}{4} ((\hat{N} - 2)^2 - \hat{E}^2) + \frac{t}{\sqrt{2}} (d_{+,\downarrow} + d_{+,\downarrow}^\dagger) \gamma_1 + \frac{\Gamma}{\sqrt{2}} \sum_k (d_{+,\sigma}^\dagger c_{k\sigma} + c_{k\sigma}^\dagger d_{+,\sigma}) \quad (\text{A.14})$$

is represented in ??

We can explain this three-peak as the result of a new strong coupling interaction characterized by the spin exchange between both dots.

In addition, the spin-up DOS at the Fermi energy grows faster than the spin-down DOS, breaking the initial spin-symmetry when $t_1 = t_2 = 0$. At $t_1 = t_2 = 0.02D$ the spin-up DOS at the fermi energy doubles the spin-down DOS which implies that the Majorana signature is present in both dots. Indeed ?? shows that the relation $\frac{\rho_{\uparrow}(0)}{\rho_{\uparrow}(0)}$ increases continuously from 1 to 2. Note that the Majorana is completely attached when the coupling t_1 reaches the order of $0.01D$.

A.3 Initial DQD-Majorana Hamiltonian.

$H_{N_\uparrow=0, P_\downarrow=-1}$:

$$\begin{aligned} |\downarrow, \downarrow, \downarrow\rangle &\rightarrow \begin{bmatrix} \varepsilon_d^+ + \frac{U^+}{2} - 2h + \varepsilon_m & 0 & -\tilde{t}_{+1} & \tilde{t}_{+2} \\ 0 & \frac{U^+}{2} + \varepsilon_m & \tilde{t}_{-2}^* & \tilde{t}_{-1}^* \\ 0, \downarrow, 0\rangle &\rightarrow \begin{bmatrix} -\tilde{t}_{+1}^* & \tilde{t}_{-2} & \varepsilon_{d_2} + \frac{U^+}{2} - h - \varepsilon_m & t \\ \tilde{t}_{+2}^* & \tilde{t}_{-1} & t^* & \varepsilon_{d_1} + \frac{U^+}{2} - h - \varepsilon_m \end{bmatrix} \\ |\downarrow, 0, 0\rangle &\rightarrow \end{aligned}$$

A.3. Initial DQD-Majorana Hamiltonian.

$$H_{N_\uparrow=0, P_\downarrow=1} :$$

$$\begin{aligned} |0,0,0\rangle &\rightarrow \left[\begin{array}{ccccc} \frac{U^+}{2} - \varepsilon_m & 0 & \tilde{t}_{+1} & \tilde{t}_{+2} \\ 0 & \varepsilon_d^+ + \frac{U^+}{2} - 2h - \varepsilon_m & \tilde{t}_{-2}^* & -\tilde{t}_{-1}^* \\ \tilde{t}_{+1}^* & \tilde{t}_{-2} & \varepsilon_{d_1} + \frac{U^+}{2} - h + \varepsilon_m & t \\ \tilde{t}_{+2}^* & -\tilde{t}_{-1} & t^* & \varepsilon_{d_2} + \frac{U^+}{2} - h + \varepsilon_m \end{array} \right] \\ |\downarrow,\downarrow,0\rangle &\rightarrow \\ |\downarrow,0,\downarrow\rangle &\rightarrow \\ |0,\downarrow,\downarrow\rangle &\rightarrow \end{aligned}$$

$$H_{N_\uparrow=2, P_\downarrow=-1} :$$

$$|\uparrow\downarrow, \uparrow\downarrow, \downarrow\rangle \rightarrow \begin{bmatrix} 2\varepsilon_d^+ + \frac{3U^+}{2} + \varepsilon_m & 0 & \tilde{t}_{+1} & \tilde{t}_{+2} \\ 0 & \varepsilon_d^+ + \frac{U^+}{2} + 2h + \varepsilon_m & \tilde{t}_{-2}^* & -\tilde{t}_{-1}^* \\ \tilde{t}_{+1}^* & \tilde{t}_{-2} & f(d_1, d_2) + h - \varepsilon_m & -t \\ \tilde{t}_{+2}^* & -\tilde{t}_{-1} & -t^* & f(d_2, d_1) + h - \varepsilon_m \end{bmatrix}$$

with $f(d_i, d_j) = \varepsilon_{d_i} + \frac{U_i}{2} + 2\varepsilon_{d_j} + \frac{3U_j}{2}$.

$$H_{N_\uparrow=2, P_\downarrow=1} :$$

$$|\uparrow, \uparrow, 0\rangle \rightarrow \begin{bmatrix} \varepsilon_d^+ + \frac{U^+}{2} + 2h - \varepsilon_m & 0 & -\tilde{t}_{+1} & \tilde{t}_{+2} \\ 0 & 2\varepsilon_d^+ + \frac{3U^+}{2} - \varepsilon_m & \tilde{t}_{-2}^* & \tilde{t}_{-1}^* \\ -\tilde{t}_{+1}^* & \tilde{t}_{-2} & f(d_2, d_1) + h + \varepsilon_m & -t \\ \tilde{t}_{+2}^* & \tilde{t}_{-1} & -t^* & f(d_1, d_2) + h + \varepsilon_m \end{bmatrix}$$